Paper III

Anders Sirevaag, Miles G. McPhee, James H. Morison, William J. Shaw and Timothy P. Stanton.

Wintertime mixed layer measurements at Maud Rise, Weddell Sea

Wintertime Mixed Layer Measurements at Maud Rise, Weddell Sea

Anders Sirevaag, Miles G. McPhee, James H. Morison, William J. Shaw and Timothy P. Stanton

Abstract

Sea ice plays a crucial role in the exchange of heat between the ocean and the atmosphere and areas of intense air-sea-ice interaction are important sites for water mass modification. The Weddell Sea is one of these sites where a relatively thin first year ice cover is constantly being changed by mixing of heat from below and stress exerted from the rapidly changing and intense winds. This study presents mixed layer turbulence measurements obtained during two wintertime drift stations in August 2005 in the eastern Weddell Sea, close to the Maud Rise seamount. Turbulence in the boundary layer is found to be controlled by the drifting ice. Directly measured heat fluxes compare well with previous studies and are well estimated from the mixed layer temperatures and mixing. Heat fluxes are also found to roughly balance the conductive heat flux in the ice, hence little freezing/melting was observed. The underice topography is estimated to be hydraulically very smooth; comparison with a steady 1-D model shows that these estimates are made too close to the ice/ocean interface to be representative for the entire floe. The main source and sink of turbulent kinetic energy are shear production and dissipation. However, the presence of a horizontal density gradient and an increasing amount of open leads are found to influence the production and sinks of turbulent kinetic energy and dynamics in the mixed layer.

1 Introduction

The Weddell Sea is considered one of the prominent sites for production of ocean deep water, both produced at the large shelf areas and by open ocean convection. The potential for the latter is caused by an often thin and weak pycnocline that separates the mixed layer from the warmer water below, a pycnocline that is easily eroded as wind induced mixing increase or convection caused by salt release from growing ice occur [*Gordon*, 1991]. Removing this pycnocline and bringing warm water towards the surface melts the ice and initiates a massive exchange of heat from the ocean to the atmosphere. The Weddell Polynya which occurred in the mid-seventies serves as a prime example of this state of extreme air-sea-ice interaction [*Carsey*, 1980; *Gordon*, 1978; *Zwally and Gloersen*, 1977]; This polynya persisted over several winters and had its origin around Maud Rise, a topographic feature in the eastern Weddell Sea centred at 65˚S 3˚E. In this area relatively warm Weddell Deep Water (WDW) flows onto the topographic feature and introduces heat and salt that can be mixed upwards and affect ice formation, stability and the fluxes of heat, salt and momentum in the surface layer [*Gordon*, 1991]. Hydrographically, the water column around Maud Rise has two distinct features; the northern and western flanks of the rise are surrounded by a halo in which the water column has a relatively high temperature maximum (T_{max} >1°C) and salinity maximum (S_{max} >34.7) and a relatively shallow mixed layer, often designated Halo water [*de Steur et al.*, 2007; *Muench et al.*, 2001]. The water column on top of the rise itself is a Taylor column with lower T_{max}, S_{max}, static stability and a deeper pycnocline, so called Taylor Cap water [*Gordon and Huber*, 1990; *Muench et al.*, 2001]. The low stability water column implies that mixing processes at the pycnocline and in the mixed layer are of great importance regionally and globally.

In recent decades, instrumentation has improved facilitating direct *in situ* measurements of turbulence and mixing. Drifting sea ice offers a convenient stable platform for such measurements. Several drifting experiments in the Weddell Sea have been conducted [*McPhee and Martinson*, 1994; *McPhee et al.*, 1996; *McPhee*, 2008a] focussing on small scale dynamics and scalar fluxes in the mixed layer. One of these experiments [ANZFLUX; *McPhee et al.*, 1996] was performed in the Maud Rise area in the austral winter of 1994 offering detailed measurements in this potentially unstable water column covered only by a relatively thin layer of first year ice. *McPhee et al.* [1996] found that heat fluxes under these conditions could be determined from mixed layer temperature elevation above freezing, friction velocity and a turbulent exchange coefficient which was more or less similar as for

heat fluxes under thick Arctic pack ice [*McPhee*, 1992; *McPhee et al.*, 1999]. Heat fluxes were on average about 27 W m^{-2}, however they showed a large temporal variation with varying atmospheric and hydrographic conditions. In addition, it was found that the underice roughness length was about two orders of magnitude smaller than for Arctic pack ice conditions, hence reducing the stress exerted on the water column by the drifting ice. The ice cover's response to wind forcing was more rapid with an ice drift/wind ratio up to twice as large as for Arctic pack ice [*McPhee et al.*, 1996], as expected for ice with relatively smooth underice topography.

Based on the potential for deep convection caused by increased salinity in the mixed layer and by nonlinear instabilities at the pycnocline [*Akitomo*, 2006; *McPhee*, 2000], a new field campaign was launched in the austral winter of 2005. The *MaudNESS* (Maud Rise Non-linear Equation of State Study) experiment was designed to make detailed observations in the upper ocean as the water column preconditioned for possible deep convection. It consisted of several phases; the first phase was a CTD survey mapping the hydrography over Maud Rise to find the areas where onset of deep convection was most likely [see *de Steur et al.*, 2007]. The second phase consisted of two ice-based drift stations where measurements of the entire upper ocean were made. In the third phase potentially unstable water masses found during the first phase were tracked and small scale measurements were made using ship based instrument systems in drifts with typical durations of one day. A central part of the design strategy for *MaudNESS* was that phase three would concentrate on rapid deployments in marginal conditions for which it might be both unsafe and untimely to put instrumentations and observers on the ice. However, deploying all the instrumentation from the ship in phase three dictated that we would be unable to make measurements in the upper part of the boundary layer. We anticipated that phase two, with direct measurements of near surface fluxes away from the disturbing influence of the ship would provide "ground truth" for estimating similar fluxes during phase three.

This paper explores phase two measurements by considering data from the two ice based drift stations during this phase, designated P2D1 and P2D2. It is organized as follows. In the next section the instrumentation will be described along with descriptions of the two drifts. In section three the general hydrographic conditions and turbulent fluxes will be presented and small scale dynamics and turbulence parameters will be analyzed, discussed and compared to a one dimensional steady state turbulence model in section four. Summary and concluding remarks are given in section five.

2 Experimental setup

2.1 Instrumentation

Central to the *MaudNESS* upper boundary layer turbulence measurements, were the Turbulence Instrument Clusters (TIC) designed to measure turbulence at a given depth below the ice. Each of these consists of a Sontek/YSI Acoustic Doppler Velocimeter (ADV), which measures three dimensional velocities in a small volume 18 cm from the tip of the instrument, combined with a fast response SBE-3 temperature sensor and a dual needle SBE-7 micro-conductivity sensor, manufactured by Sea-Bird Electronics. The micro-conductivity sensor (hereinafter referred to as µC) is designed to capture rapid changes in conductivity and will, combined with the temperature measurements, provide fluctuations in salinity. In addition, a standard SBE-4 conductivity cell, also from Sea-Bird Electronics, is included to provide stable measurements of the salinity over a wide range of spatial scales. All sensors, except the SBE-4 conductivity cell (subsequently referred to as stdC), are mounted in the same horizontal plane, making it possible to combine measurements to calculate vertical fluxes at a given depth below the ice. The stdC sensor was mounted about 20 cm above the others to prevent disturbance of the flow field. During *MaudNESS*, TICs were mounted on vertical masts in two configurations; the so-called shallow mast contained one TIC and was deployed directly through the ice with an orientation directed manually into the mean flow relative to the ice. The mid-level turbulence mast supported two TICs mounted with a vertical spacing of 4 m making flux measurements at two levels possible. Only the upper one of these included a micro conductivity sensor. The main difference between the two masts is that the shallow mast was suspended using rigid poles fixed to the ice, while the mid-level mast was suspended by a wire, allowing it to rotate freely in the water column. In this study turbulence measurements mainly from the near surface layer, which include data from the mid-level mast during P2D1 and data from the shallow and mid-level mast during P2D2, are presented and discussed.

The ship was equipped with a 150 KHz acoustic doppler current profiler (ADCP) which supplied profiles of horizontal velocity averaged over a period of 5 minutes and in depth bins of 8 m, from 35 m below the surface and with good quality at least throughout the mixed layer. Velocities from the ADCP were corrected for the ship movement and oriented relative to true north. However, the measurements from the ship mounted ADCP can be distorted by ice along and under the hull of the ship, which unfortunately happened in some

periods during P2D2. A second profiling instrument, a Sontek Acoustic Doppler Profiler (ADP) was additionally deployed nearby the shallow mast during P2D2. When deployed from the ice, this ADP can provide measurements relatively close to the surface, an advantage compared to the ship mounted ADCP. The ADP was deployed less than 1m below the ice, looking downward and set to measure current velocity in 20 depth cells, each with a vertical extension of 2 m. After adding the instrumental blanking distance of 1m, the first depth cell in the velocity profile was centred at 3m. The ADP measures three dimensional velocities, referenced to magnetic north using the internal compass, along with the strength of the returned signal. The latter, after subtracting the background noise signal, defines the signal-to-noise ratio.

In addition to the temperature and salinity measurements provided by the TICs, a automated cycling CTD was deployed from the ship during every drift and this was used to gain information about the mixed layer hydrography. A relatively high sampling rate of about one profile every 10 minutes, provided high temporal resolution of the temperature and salinity fields.

The ship's data acquisition system included measurements with a variety of different sensors in addition to the ship mounted ADCP. This study utilizes position data from the ship's GPS system plus air temperature and wind measurements made 17 m and 32 m above sea level. Wind speed measurements from 17 m height were adjusted to 10 m values following *Smith* [1988].

2.2 Drift descriptions

The first phase two drift, P2D1, took place over the eastern half of the Maud Rise seamount, August 9th 4pm – August 11th 8am. Drift P2D2 was over the western flank of the seamount, August 12th 3pm – August 16th 10pm. Hereafter the time convention yearday will be used, where day 1 corresponds to January 1st 2005 and August 9th 2005 is yearday 221. Fig. 1 shows the trajectories of both drifts plotted on top of the bathymetry of Maud Rise.

The GPS data were used to obtain continuous ice drift velocity and position data for the two drifts. One-second position data were transformed into local x and y coordinates in a polar stereographic grid, rotated with the x-axis along 90˚E and y-axis along 0˚E and centred with origin at 65˚S 3˚E, corresponding approximately to the centre of Maud Rise. For every 20 minutes, x and y data are transformed to a complex vector and fitted to a second order complex polynomial in time within the interval. The velocity is taken as the derivative of this

at any time. Since the ship was moored to the floe during the drift periods, the calculated ship velocity is equal to the ice drift velocity.

The first drift, P2D1, was established at initial position 64.81˚S 2.87˚E under windy conditions and on relatively small ice floe consisting of flat first year ice. A survey performed on day 222, determined the average ice thickness to be 39 cm with an average snow layer of 7 cm. These thicknesses were measured along a transect of about 300m, counting 23 individual measurement points (D. Notz and D. Goldberg, pers. comm., 2005). The floe drifted north-east 67.56 km over a period of 38 hours, equivalent to a mean drift velocity of 49.4 cm/s. Drift velocities calculated from the ship GPS data had a maximum and minimum of 70.5 cm/s and 22.2 cm/s, respectively.

Weather conditions during P2D1 were set by a low pressure system positioned south of Maud Rise for most of the drift period. This resulted in relatively low temperatures and strong winds which were close to westerly; average wind direction was 259 degrees. The wind speed had maximum and minimum values of 17.3 ms^{-1} and 8.8 ms^{-1}, respectively; average wind speed was 13.3 ms^{-1}. Air temperatures in the drift period varied between -24.3°C and -13.7°C with an average temperature of -19.6°C.

The mid-level turbulence mast was deployed from time 221.9, levelled close to the ice with the upper TIC at 2.8 m depth and the lower at 6.8 m to make measurements in the surface layer. Unfortunately, unstable ice conditions forced a rapid recovery of all instrumentation on the ice, including the middle mast at time 222.75. The cycling CTD, which was deployed from the ship, started the measurements at time 222.6 and kept measuring until the end of the drift, day 223.3.

After the end of the unstable P2D1, a vast and initially more solid floe was found for the second drift, P2D2. This drift started out on the evening of day 224 at initial position 64.58˚S 0.67˚E and the floe consisted of relatively flat ice with some small ridges and some rafted ice observed at the surface. Measurements along a 300m long transect revealed variations in ice thicknesses between 20 cm and 80 cm with an average ice thickness of 40 cm and no significant melting or growth of ice was observed during the drift. A layer of snow averaging 14 cm thick was present on the ice (D. Notz and D. Goldberg, pers. comm., 2005). Instruments were deployed throughout the evening of day 224 and most of the upper boundary layer instruments were operating from day 225.1. The shallow turbulence mast was deployed at 2.8m below the ice about 300m from the ship. The mid-level turbulence mast was deployed closer to the ship at about 30 m depth. The ADP was deployed at the same location as the shallow mast. At time 226.82 a crack divided the floe in two and forced a recovery of

the instruments farthest away from the ship. Redeployment of the shallow mast and the ADP were done close to the mid-level turbulence mast, about 50m from the ship. Most instruments operated again from 227.5 and until the end of the drift.

The drift P2D2 (Fig. 1) started northward, making a sharp turn at time 226.3, then drifting southeast, turning clockwise and after another sharp turn on day 228.6 ending up northward again towards the end of the drift on the evening of day 228. Net drift over the period of 92 hours was 28.81 km with a mean direction of 241.2 degrees; however the total drifted distance was 71.91 km, equivalent to a mean drift speed of 21.7 cm s^{-1}. From the GPS data, maximum and minimum ice drift speed, as calculated from the GPS data were 38.1 and 1.0 cm s^{-1}.

The longer lasting P2D2 offered calmer wind conditions, but the wind pattern was more varied which is reflected in the more complex drift trajectory. The average wind speed was 7.8 ms^{-1} with a maximum of 11.2 ms^{-1} and a minimum of 3.2 ms^{-1}. Initial wind direction was southerly on day 225, during the drift the wind made a complete 360 degrees clockwise rotation in direction, turning back to southerly again during day 228. Mean temperature over the period of the drift was -18.0°C, maximum and minimum temperature was -14.7°C and -21.9°C, respectively. The atmospheric conditions during the drift was the result of a high pressure system passing by the ship with maximum pressure at time 226.2 and then passing of a low pressure system with stronger winds and minimum pressure at time 227.7. Temperature minimum and maximum also occurred at the times of maximum/minimum air pressure.

3 Measurements

3.1 *Mixed layer hydrography*

Fig. 2 and Fig. 3 show the mixed layer depth, mean mixed layer temperature and mean mixed layer salinity for both drifts, all extracted from the cycling CTD data. The mixed layer depth is determined as the depth where the salinity exceeds the upper layer mean salinity (50 – 60 m for P2D1 and 20 – 30 m for P2D2) by 0.02 psu (following the approach of *de Steur et al.* [2007]) and the mixed layer temperatures and salinities are averages of all measurement points above the mixed layer depth.

The first drift was in the Taylor Cap water over the northeast side of the rise and conditions encountered there fit into previous descriptions with a cold mixed layer over a relatively deep pycnocline. Mean mixed layer temperature, salinity and depth was -1.81°C,

34.46 and 123 m, respectively. Mixed layer depth increased from initially 105 m to 150 m towards the end of the drift. In the same period the mixed layer got slightly colder and fresher, indicating that changes in mixed layer properties were probably due to horizontal gradients as we drifted eastward and not due to mixing across the pycnocline which would make the mixed layer warmer and saltier. Temperatures and salinities from TIC measurements at 2.8 m and 6.8 m depth are also plotted. Although the overlapping period of data from the TIC and cycling CTD was quite short, it shows that there was a surface layer slightly colder and fresher than the mean mixed layer.

P2D2 took place on the flank of the Maud Rise in the transition region between Halo Water and Taylor Cap Water. This is clearly reflected in the mixed layer hydrography during P2D2, as we drifted from the Halo Water, into Taylor Cap Water and then slowly into the Halo Water again (In Fig. 3A, periods meeting the Halo Water criteria, $T_{max} > 1°C$, $S_{max} > 34.7$ [*de Steur et al.*, 2007], are marked with a thick horizontal line). These transitions are reflected as relatively large variations in mixed layer depth, temperature and salinity. Mixed layer depth varied from 80 m to 20 m with a mean value of 37 m and, the mixed layer was in general warmer during P2D2 with a mean temperature of -1.66°C, but instantaneous temperatures as high as -1.2°C were encountered during the drift. Increase in temperature was followed by a decrease in salinity in the Halo water; average salinity was 34.48 for the whole drift. Temperature and salinity measurements from the TIC at 2.8 m are also plotted in Fig. 3B and Fig. 3C and water properties at 2.8 m in general followed the mixed layer conditions, meaning that the mixed layer was truly well mixed. Though not so much as P2D1, the P2D2 mixed layer was slightly more stratified in the Halo water, where the upper mixed layer was colder and fresher than the rest of the mixed layer. This might indicate that mixing of heat from the underlying warm waters and into the pycnocline was not complete, alternatively that a new shallower mixed layer had developed within the original mixed layer.

The temperatures of the mixed layer during the second drift were also well above freezing, indicating that there were relatively large amounts of heat available for mixing towards the ice/ocean interface.

As will be discussed, Fig. 3 reveals that relatively large temporal variations in hydrography were encountered along the drift. In general, there is always a question whether the encountered horizontal gradients conflict with the general assumptions of horizontal homogeneity in turbulence analyses.

3.2 Mixed layer currents

During P2D1 a general picture of the flow conditions in the upper mixed layer was provided by the ship mounted 150 KHz ADCP, which covered the mixed layer below 35 m depth and the TIC situated 2.8 m below the ice/ocean interface. Ship ADCP data were post processed by the University of Hawaii and made available as 5 min averages representing velocities averaged in 8 m depth bins. Velocities from the TIC were averaged in one hour bins and the directions of the mean flow were adjusted by the magnetic declination, which in the Maud Rise region was 21°W. The TIC measures velocities relative to the ice, so in order to obtain the absolute velocities the ice drift velocity vector was added to the relative velocity vector. In Fig. 4 hourly averages of the northerly and easterly components of currents at 2.8m and 35m are shown together with the components of ice drift and wind. Figure shows that the upper mixed layer oscillate in phase with the ice with a period close to the inertial period of 13.4 hours. At both 2.8 m and 35 m absolute current velocities are well correlated with the ice velocity (correlation coefficients above 0.7). Average current speed was 12 cm s^{-1} at 35 m and 18 cm s^{-1} at 2.8 m, while the average ice drift speed was 49 cm s^{-1}. This shows that most of the velocity shear is in the upper meters of the mixed layer and that there was also an angular shear in the mixed layer; Currents at 2.8m was directed 9 degrees to the left of the ice drift. Below the pycnocline, ADCP velocities centred at 147 m (not shown here) showed mean velocities of 3 cm s^{-1} and variations at the M_2 frequency, which corresponds well with the modelled estimates of the barotropic tide in Maud Rise region [*Robertson et al.*, 1998].

During P2D2, the ADP was deployed from the ice and the velocity profiles from the ADP were processed as follows. First the velocity was rotated into an East-North-Up coordinate system using the internal compass giving the direction of the magnetic north. Then all profiles were averaged in 1 hour bins. The quality of the measurements was checked by the magnitude of the signal-to-noise ratio and all measurements with values above 5dB are considered of good quality. The depth range of the ADP was detected as the lowest depth cell where the signal-to-noise ratio was never lower than 5dB during the time of deployment, which during P2D2 was 29 m. As with the TIC data, the ADP measures directions with the internal magnetic compass and directions were corrected using the local magnetic declination. After the adjustments, absolute velocities were found by subtracting the ice velocity vectors.

The second drift had more complex wind and current conditions, but again inertial (or semidiurnal tidal) oscillations were a prominent feature of mixed layer velocities. (Fig. 5). At 29 m, mean velocity was 6 cm s^{-1}, while mean current velocity at 2.8 m was 7 cm s^{-1}. Also

during P2D2 most of the velocity shear was in the upper meters of the mixed layer. The angular shear in the mixed layer can be measured using the high frequency ADP which can offer, unlike the ship ADCP, a relatively high vertical resolution in the upper 30 m. Data from the ADP shows a distinct Ekman-turning of current velocity in the upper 30 m, with a mean turning of 12.3°. (see also section 4.4, Fig. 11). As for the first drift, current velocity at 2.8 m is well correlated with the ice drift velocity with a correlation coefficient of 0.74. However, velocities from the ADP at 29 m are uncorrelated with the ice velocities indicating that only the upper part of the mixed layer is oscillating in phase with the ice. The most likely explanation for this is the relative rapidly changing hydrography during this drift setting up horizontal density gradients resulting in baroclinic flows. Such flows were found to be present in the area of P2D2 and are discussed in further detail by *de Steur et al.* [2007].

3.3 Turbulence

Turbulence and turbulent fluxes were calculated from the TIC measurements at 2.8 m below the ice/ocean interface. The exception was the P2D1 drift where a frozen conductivity sensor excluded any salt flux estimate from the 2.8 m TIC and therefore salt fluxes from the 6.8 m TIC were used instead.

Under sea ice, turbulent energy containing eddies often persist for up to several minutes. Choosing an averaging interval of 15 minutes for the turbulence statistics, assure us of capturing the covariance in the turbulent eddies but avoid including energy contributed by other processes with variability on a larger time scale. Within each of the 15-minutes realizations, velocities are rotated into a streamline coordinate system aligned with the x-axis along the mean current, so that the mean along stream component is equal to the mean velocity and the mean cross stream and vertical components vanish. Deviatory quantities of velocity, temperature and salinity are obtained by linear detrending within each 15-minute realization before the Reynold stress and fluxes of heat and salt are calculated according to

$$\tau = \langle u'w' \rangle + i \langle v'w' \rangle \tag{1}$$

$$F_H = \rho c_p \langle w'T' \rangle \tag{2}$$

$$F_S = \langle w'S' \rangle \tag{3}$$

In (1) − (3), τ is the horizontal kinematic Reynolds stress, from which the local friction velocity is calculated as $u_* = |\tau|^{1/2}$. u', v', and w' are the three deviatory velocity components, F_H and F_S are heat and salt fluxes, respectively, ρ is the mixed layer density, c_p is the specific heat of sea water. T' and S' are the deviatory temperature and salinity and brackets indicate 15 - minute means. To remove some of the natural variability between every realization, flux estimates are averaged in 1 hour bins for P2D1 and 3 hours bins for P2D2. TIC measurements are made in the so called constant flux layer below the ice and fluxes calculated at 2.8 m depth are considered to be interface values. For P2D2, also measurements from the mid-level mast are shown. Technical problems with some of the sensors on the mid-level mast prevented us from getting data from the entire P2D2 drift period, but a 24 hours time span of data from 30.6 m depth are included.

Calculated friction velocities and fluxes of heat and salt from P2D1 are shown in Fig. 6 and mean values are summarized in Table 1. The friction velocity had an average value of 0.98 cm s^{-1}; however the surface stress was increasing steadily during the whole drift, following the increasing wind and drift velocity. Friction velocities were relatively low considering the large drift velocities and thus reflected the relatively smooth underside of first year ice compared with multiyear pack ice in the Arctic [*McPhee*, 2002] and western Weddell Sea [*McPhee*, 2008a]. The observations are also in line with other observations from the Weddell Sea, reporting similar values of friction velocity under similar conditions [*McPhee et al.*, 1999].

The turbulent heat flux towards the ice/ocean interface was positive for more or less the whole drift with heat fluxes in the range from 0 to 27 W m^{-2}. Average heat flux was 13.8 W m^{-2}. During the ANZFLUX Maud Rise Drift in 1994, the average heat flux was 23.4 W m^{-2} in almost the same location and at the same time of year [*McPhee et al.*, 1999].

The u_* records for P2D2 (Fig. 7) show that the second drift was not as dynamically energetic as the first drift. This was due to smaller drift velocities, average friction velocity was 0.56 cm/s, about half of the value for P2D1, but also reflecting a smooth underice topography. However, the heat and salt fluxes were greatest at the second drift. Heat fluxes were always positive during P2D2, ranging from 1.2 W m^{-2} to 82.2 W m^{-2}. Mean upward heat flux was 28.0 W m^{-2}. The elevation of the mixed layer temperature above freezing (Fig. 7) shows that there was more heat available for mixing during P2D2 compared to P2D1, which is reflected in the higher heat fluxes. P2D2 also displayed a larger temporal variability in

mixed layer temperature, salinity and ice drift velocity which resulted in larger variability in the interface fluxes.

Turbulent salt fluxes were captured using the μC sensor on the TIC. However, there are some drawbacks using these sensors. First they are subject to a considerable drift in absolute conductivity over time; and second, the needle construction of the sensor itself makes it susceptible for biofouling which often introduce spurious jumps in the resulting salinity signal. In order to fix the first problem, absolute conductivity from the stdC cell at same depth is used to adjust the mean μC to the ambient conductivity. The second problem is solved by removing periods in the data sets where these jumps in conductivity occur, eliminating the risk of introducing large, erroneous salt fluxes. Both these fixes were applied to the P2D2 salt fluxes, however for P2D1 the stdC sensor at 2.8 m failed, so for P2D1 salt fluxes from the stdC sensor at 6.8 m is presented.

The stdC sensor is designed with a glass duct which the water flows through. When the water is not pumped through this duct, the flow velocity in the duct is set by the surrounding flow and from fluid dynamics the flow in the duct is smaller than outside [e.g. *Morison et al.*, 1994]. This reduced flow has a low pass filtering effect on the conductivity sampling, hence this sensor is not able to capture all the salinity variance in the turbulent flow. In terms of salt fluxes, *McPhee and Stanton* [1996] estimated that by using the stdC sensor they could capture up to 70 % of the salt fluxes captured using the μC sensor. The shallow turbulence mast was manually aligned towards the mean flow, which means that with changing current or drift directions, periods did occur when the mean flow was not directed straight towards the stdC sensor. With a smaller velocity component along the stdC main axis, the duct flow will be further reduced and the low pass filtering of conductivity will be enhanced. Salinity is calculated from conductivity and temperature and in order not to introduce artificial variance in the salinity signal, temperature must be low pass filtered before calculating salinity and covariance fluxes. In addition, a quality criterion that the mean flow should not be directed more than 30 degrees off the main stdC axis, was applied before calculating salt fluxes from the stdC sensor. For the P2D2 shallow mast, about 60 % of the 15 minutes averages met this criterion. For the rest of this paper, salt fluxes from 2.8 m during P2D2 refer to fluxes from the μC sensor, however stdC fluxes are plotted in Fig. 7 and mean values are given in Table 2 to be able to compare the fluxes for periods where the mean flow had the orientation preferable for stdC salt fluxes. The mid-level mast was not attached to the ice and rotated freely, always directing the TIC towards the mean flow. Hence, stdC salt fluxes from the mid-level mast are not subject to the same uncertainty.

Mean TIC salt fluxes were $2.1 \cdot 10^{-8}$ psu m s^{-1} for P2D1 and $-3.9 \cdot 10^{-6}$ psu m s^{-1} for P2D2. In general, a negative salt flux at the interface is related to freezing and a positive flux is related to melting. Following that, the P2D1 flux is too small as to indicate a significant change in ice thickness, whereas the P2D2 salt fluxes, calculated from μC sensor, represents freezing of 3.6 cm of new ice during the whole drift period (assuming an ice salinity of 10 psu).

For the mid-level mast in the period 227.75 to 228.63, mean values of friction velocity, heat flux and salt flux were 0.39 cm s^{-1}, 20.7 W m^{-2} and $4.6 \cdot 10^{-6}$ psu m s^{-1}, respectively. The most distinct feature of the measurements at 30.6 m depth was the shift in heat flux around 228.3, where fluxes go from negative (mean ~ -9 W m^{-2}) to large positive (mean ~ 71 W m^{-2}).

4   Discussion

4.1 Dynamics of the ice drift

The drift of the ice was clearly controlled by the wind and modulated by oscillations at the inertial frequency. Using the complex demodulation technique of *McPhee* [1990] complex position data are fitted to a function containing a mean velocity and oscillating clockwise and counter clockwise components at the inertial and diurnal frequencies. The function is fitted to the data over one diurnal period (one day) and the function coefficients are evaluated every three hours.

As stated from Fig. 4 and Fig. 5, the ice drift exhibited inertial oscillations and by separating the total ice drift velocity into inertial (and diurnal) components and a mean component, we are able to examine the mean ice drift velocity compared to wind velocity. By considering only periods where wind speeds are larger than 4 m s^{-1} (100 % and 92 % of time for P2D1 and P2D2, respectively) we find the ratio of mean ice drift velocity to 10-m wind speed to be 3.7 % and 2.6 % for P2D1 and P2D2, respectively. In general the drift directions were to the left of the wind, on average 16° for P2D1 and 9° for P2D2. The wind induced drift is close to previously reported values for winter time conditions and thin first year ice in the Weddell Sea. *McPhee et al* [1996] reported ice drift speeds of 3.1 % and 3.8 % of the wind speed and ice drift direction about 15° to the left of the wind for the 1994 ANZFLUX study. Similar studies in 1986 by *Martinson and Wamser* [1990] also presented ice drift with

velocity magnitudes 3.0 % of wind speed (3.2 % after adjusting to 10 m wind [*McPhee et al.*, 1996]) and ice drift 23° to the left of the wind.

Mean ice drift and wind velocity are also highly correlated (correlation coefficients 0.82/0.88 for P2D1/P2D2) which confirms that ice was drifting freely with the wind.

4.2 Ice/ocean interface fluxes

When considering the ice/ocean heat balance, one has to know the conductive heat flux in the ice. For P2D1, only ice and snow thicknesses were measured, during P2D2 ice/snow interface temperatures were measured in addition to the thicknesses.

The measured ice and snow thicknesses of P2D1 (section 2.2) are used to estimate the conductive heat flux in the ice and snow, assuming there was a linear temperature gradient through the ice and snow set by the mean atmospheric temperature and the mean mixed layer temperature. Further assuming the thermal conductivity of snow and ice to be 0.15 W K^{-1} m^{-1} [*Sturm et al.*, 1997] and 2.1 W K^{-1} m^{-1} [*Trodahl et al.*, 2001], respectively, leads to an average conductive heat flux of 24 W m^{-2}. This is close to twice the average ocean heat flux and indicates that there was input of latent heat from freezing at the interface to balance the heat fluxes. The amount of latent heat was roughly equivalent to the freezing of 0.4 cm of ice during the period of the measurements (using latent heat of fusion for sea ice with temperature -2°C and salinity of 10 psu). This freezing should result in an average salt flux into the ocean of about -1.5·10^{-6} psu m s^{-1}. The measured salt flux differs from this estimate, both in magnitude and sign. There are several factors contributing to this discrepancy: i) The conductive heat flux estimate is very rough ii) The stdC sensor does not capture all the covariance in the flow iii) The measurements at 6.8 m do not represent the interface conditions but are rather the result of flux through an underlying salinity gradient as indicated in Fig. 2C. To follow up iii), we estimate the salinity gradient in the overlapping period of P2D1 (222.6 to 222.8) from the mean mixed layer salinity and salinity at 2.8 m to be -2.5·10^{-4} psu m^{-1}. Setting diffusivity of salt equal to the calculated eddy viscosity, $K_S = K_m = 0.0081$ results in an upward salt flux of 2·10^{-6} psu m s^{-1}. This salt flux is of the same order as the estimated salt flux from freezing at the interface but with opposite sign and shows that the surface stress combined with background salinity gradient overpowers the surface salinity flux from freezing and hence the measured salinity flux is small.

On the second drift, the conductive heat flux was calculated in a similar way, except that the ice/snow interface temperatures were used to calculate temperature gradients in the

ice only. This way the uncertainties related to the thermal conductivity of snow and the assumption that the surface temperature was equal to the air temperature can be avoided. The repeated measurements indicated that the ice thickness remained more or less constant throughout the drift. Based on the temperature measurements at the ice/snow interface and the mean water temperature of -1.70°C at 2.8 m depth below the ice, temperature gradients are calculated leading to an estimate of the conductive heat flux in the ice. This flux remained more or less constant at around 40 W m^{-2} when averaged over the three transects made during the drift. The conductive heat flux was about 10 W m^{-2} larger than the average ocean heat flux and to obtain flux balance at the interface, a total ice growth of 1.2 cm during the 92 hours of the drift is required. When measuring the temperature at the ice/snow interface, a removal of the snow in the proximity of the measuring spot will lead to a cooling of the ice surface and the measured temperature will be lower than the actual interface temperature. This leads to an overestimation of the temperature gradient in the ice and hence to a larger conductive heat flux, leaving the estimated ice growth as an upper limit. In any event, the estimated ice growth was below the threshold for what was possible to measure, at least when the large horizontal variability in ice thicknesses is considered. Following the previous simplified thermodynamic calculations, an estimated ice growth of 1.2 cm over the period of the drift is equivalent to a salt flux of -1·10^{-6}, which is about three times less than salt fluxes we measured with the μC sensor. This discrepancy might indicate that other processes than freezing/melting at the interface contributed to the salinity variance.

For both drifts, heat and salt fluxes at the ice/ocean interface showed reasonable values compared to mean values of conductive heat fluxes in the ice. And since we lack a higher temporal resolution in ice measurements, we do not know how melting or freezing changed during the drifts.

Previous studies have shown that the heat flux in the mixed layer under drifting sea ice can be related to the product of interface friction velocity (u_{*0}) and the temperature elevation above freezing (δT) via the turbulent transfer coefficient (c_H) [E.g. *McPhee*, 1992].

$$\langle w'T' \rangle = c_H u_{*0} \delta T \tag{4}$$

This transfer coefficient has shown to be remarkably constant for a large variety of ice and hydrographic conditions [E.g. *McPhee*, 1992; *McPhee et al.*, 1999] and *McPhee et al.* [2008] recommends $c_H = 0.0057$ based on data from several Arctic and Antarctic experiments.

For each drift, the turbulent exchange coefficients were calculated by linear regression through the origin of $\langle w'T' \rangle$ against $u_* \partial T$ for all the 15-minute intervals (81 and 252 for P2D1 and P2D2, respectively). For P2D1, heat fluxes gave an exchange coefficient of 0.0059 ± 0.0006, indicating the mean and the 95 % confidence interval, which is in the same range as previously cited studies. Similarly, for the P2D2 data, the overall exchange coefficient was 0.0069 ± 0.0004, slightly higher than the estimate from literature. In case of P2D2, the redeployment (after day 227.5) initiated a period where heat fluxes were higher than one would predict with a coefficient of 0.0057. Therefore two different coefficients were calculated for P2D2, one before and one after the redeployment. The resulting coefficients for these periods are 0.0059 ± 0.0005 and 0.0083 ± 0.0004, respectively. We explore possible explanations for the enhanced exchange in section 4.5.

4.3 Mixing length, under-ice roughness and TKE balance

Turbulent exchange can often be characterized by a velocity scale and a length scale representing the distance (mixing length, λ) over which the most energetic eddies are effective at transporting momentum. Previous studies have shown a close association between λ with the inverse of the peak at the weighted variance spectrum of vertical velocity [*McPhee and Martinson*, 1994; *McPhee*, 2008a].

For the TIC data, wavenumber spectra of vertical velocities are calculated for every 15-minute interval and spectral estimates are smoothed and averaged in wave number bins. Hourly averaged spectra are then used for calculation of the mixing length using

$$\lambda = \frac{c_\lambda}{k_{max}} \tag{5}$$

where k_{max} is the wavenumber at the peak of the weighted spectrum and c_λ is a constant, found empirically to be 0.85 [*McPhee*, 1994]. In a neutrally stable boundary layer, there is an established relation between an upper limit for the mixing length and distance from the ice/ocean boundary, $\kappa|z|$, where $\kappa = 0.4$ is the Von Karmans constant and z is the vertical distance from the interface. Further away from the boundary, the mixing length is limited by the planetary length scale, $\frac{\Lambda_* u_*}{f}$, where u_* is the local friction velocity, f is the local

Coriolis parameter and Λ_* is a similarity constant set to 0.028 [*McPhee et al.*, 1999]. Generally, the maximum mixing length is set to be the smallest of the two length scales. When buoyancy flux is significant in the turbulent kinetic energy equation, an additional scale combining stress and buoyancy flux (the Obukhov length) also plays a role.

In Fig. 8 and Fig. 9, empirical estimates of mixing length based on (5) for both drifts are plotted; mean values at 2.8 m below the ice were 0.86 m and 0.76 m for P2D1 and P2D2, respectively. For both drifts where TIC measurements were made 2.8 m below the ice, $\kappa|z| = 1.1$ m and for most of the time this was smaller than the planetary length scale, except in some periods of low friction velocities. In Fig. 10, mixing length is averaged in friction velocity intervals of $1.5 \cdot 10^{-3}$ ms^{-1} and plotted against friction velocity together with the geometric and planetary length scales. Indeed, the mixing length usually was limited by the distance from the interface, however, there also seems to be a decrease in mixing length for smaller values of friction velocity, indicating, as also argued by *McPhee* [2008a] that the planetary length scale was limiting. Hence, both the geometric and planetary length scales were important under the encountered conditions. Towards the end of P2D2 mixing length was greater than the geometric length scale, suggesting that destabilizing buoyancy fluxes were introduced, which increased the maximum mixing length towards the scale set by the Obukhov length.

The underice roughness length is related to the ratio of mean velocity and friction velocity by the "law of the wall" (LOW)

$$\frac{U(z)}{u_*} = \frac{1}{\kappa} \ln \frac{|z|}{z_0} \tag{6}$$

where z is the measurement depth. Using hourly mean values of U/u_*, z_0 is estimated to be of order $1.0 \cdot 10^{-6}$ m and $1.3 \cdot 10^{-5}$ m for P2D1 and P2D2, respectively. These values are very small and confirm the "super-smooth" conditions that were deduced from the low surface stress in section 3.3. Surface roughness calculated from LOW is actually smaller than it would be for a hydraulically smooth surface, estimated from surface stress and molecular viscosity $z_0 = (\frac{\upsilon}{u_{*0}})e^{-2}$ [*Hinze*, 1959], which gives values of $1.9 \cdot 10^{-5}$ m and $2.4 \cdot 10^{-5}$ m for P2D1 and P2D2, respectively. This indicates that the LOW might not be the best way to address the measurements at 3 m and effects of the local underice topography might affect the surface roughness calculations. Other studies [*Crawford et al.*, 1999; *McPhee*, 1990; *McPhee et al.*,

2008] have shown that the underice flow can be well estimated using Hinze's approximation of surface roughness; however in our case this is not appropriate either. To examine if the calculated surface roughness is representative for the entire floe, the problem is addressed using a steady state 1-dimensional model (section 4.4).

In a steady state turbulent flow, a simplified balance of turbulent kinetic energy is

$$P_S + P_B = \varepsilon \tag{7}$$

when divergence of TKE and pressure velocity covariance is neglected. Here, the production due to shear, P_S and buoyancy, P_B are balanced by dissipation rate of TKE, ε. The shear production can be calculated as

$$P_S = \frac{u_*^3}{\lambda} \tag{8}$$

using the mixing length obtained from eq. (5). Dissipation rate was calculated as follows. Using hourly averaged weighted spectra of vertical velocity, the inertial subrange was identified as the wave number band where the slope was -2/3 (equivalent to the -5/3 slope in unweighted spectra). If a distinct subrange existed, dissipation was calculated according to

$$\varepsilon^{2/3} = \frac{3}{4\alpha_\varepsilon} S_{ww} k^{5/3} \tag{9}$$

In (9), values of wavenumber and spectral density, k and S_{ww}, are from the inertial subrange and α_ε is a constant of 0.51 [*Edson et al.*, 1991]. Buoyancy production is defined as

$$P_B = -\langle w'b' \rangle = -g\left(\beta_S \langle w'S' \rangle - \beta_T \langle w'T' \rangle\right) \tag{10}$$

following the sign convention of e.g. *McPhee and Morison* [2001], g is the gravity constant and β_S, β_T, $\langle w'S \rangle$ and $\langle w'T' \rangle$ are the saline contraction coefficient, thermal expansion coefficient, salt flux and kinematic heat flux, respectively. Salt fluxes were relatively small during both drifts, so buoyancy production is expected to be negligible in the budget of the TKE. For P2D1 and P2D2, overall mean buoyancy production values were three and two, respectively, orders of magnitude smaller than shear production and dissipation. This

generally justifies neglecting this term as a significant factor in the TKE budget. TKE terms are plotted in Fig. 8 and Fig. 9. For the first drift, the average shear production was $1.5 \cdot 10^{-6}$ m^2 s^{-3} which was balanced by the mean dissipation rate of $2.0 \cdot 10^{-6}$ m^2 s^{-3}. The shear production increased towards the end of the drift, together with surface stress and friction velocity. Also for the second drift, the average shear production ($3.7 \cdot 10^{-7}$ m^2 s^{-3}) nearly balanced the dissipation rate ($5.1 \cdot 10^{-7}$ m^2 s^{-3}). Buoyancy production was not negligible for all of P2D2 and during the second part of P2D2 shear production was persistently less than the dissipation. In this period the μC sensor also showed a significant negative salt flux. This salt flux is equivalent to a buoyancy production that accounts for about 25 % of the discrepancy between shear production and dissipation. During this period with a large negative salt flux (day 227.5 – 228.5), there was a significant mean downward vertical velocity of 1.2 cm s^{-1} (see Fig. 15). Although these vertical velocities are too small compared to the horizontal velocities to be any free convective events, they might indicate that some processes of convective nature are present. There are several mechanisms that can result in such salt fluxes: i) Salt release from ice due to freezing ii) Convective plumes of salty brine from warm ice, as described in *Widell et al.* [2006] and iii) Convective mixing resulting from differential advection of a horizontal density gradient or cooling/freezing in open water upstream of measurement site. Points i) and ii) can be ruled out as the freezing of new ice was not significant and there was no warming events during the drift that could initiate the salt release as observed in *Widell et al.* [2006]. The observed horizontal changes in density make the differential advection a likely candidate as a source of TKE which will be discussed in section 4.5. Also, towards the end of P2D2, the ice cover was separating more and more and our floe was surrounded by an increasing amount of open water. Leads are areas of cooling and convection, hence a significant source of TKE production. The increasing closeness of convecting leads violates the assumption of horizontal homogeneity, as TKE produced upstream of the measurement site will advect with the mean flow and an excess rate of dissipation rate will be observed locally.

4.4 Steady model comparison

As presented earlier, velocity and surface stress measurements indicated that the ice underside was "super-smooth" differing from earlier observations of drifting first year ice in the Weddell Sea. The horizontal footprint of undersurface roughness elements contributing to hydraulic roughness depends on both u_* and the distance from the boundary, hence

measurements near the boundary may not adequately represent z_0 typical of the entire floe [e.g. *McPhee*, 2002]. In this section we utilize a one-dimensional, steady state, local turbulence closure model (SLTC) to characterize "floe-scale" surface roughness, and as a tool to supplement measurements in the data analysis.

The model is described in detail in e.g. *McPhee* [2008b] and is set up for this study with 160 vertical levels, spanning 80 m in vertical. The model is forced with the measured horizontal velocity at a specified depth and the actual profiles of temperature and salinity. In addition, parameters such as under-ice roughness, exchange coefficients at the interface and ice and snow thickness are specified. Based on the initial temperature and salinity in the mixed layer and the interface stress (calculated from ice drift), an initial guess of eddy viscosity is made. This is used for calculating turbulent fluxes which again will affect the eddy viscosity which then is recalculated. This iteration process is continued until the modelled velocity fits the measured velocity at the specified depth.

During P2D2 there were TIC, ADP and cycling CTD measurements from the entire period, which offers the possibility of setting up the model for the actual conditions and compare with measured turbulent fluxes and mixed layer velocity profiles.

For P2D2, measured temperature and salinity profiles and ADP velocities were averaged in 3 hour bins and the model was run separately for each interval, providing a time series of steady state variables. By matching the modelled velocity to the measured velocity at 20 m, we are far enough from the surface to represent the floe in general. The underice roughness is set to the value inferred from measurements, $z_0 = 1.3 \cdot 10^{-5}$ m. Conductive heat flux in the ice is specified to 40 Wm^{-2} and snow and ice thicknesses are set to 0.14 m and 0.40 m, respectively.

As a first check the measured velocity profile is compared with the modelled. In Fig. 11, average measured velocities from 3 m to 29 m are non-dimensionalized by the velocity at 29 m and plotted together with the equivalent modelled velocity profile for two different values of z_0. Using $z_0 = 1.3 \cdot 10^{-5}$ m as inferred from the TIC measurements clearly underestimates the angular turning of velocity observed in the upper 29 m, and in order to reproduce the observed turning a larger $z_0 = 4 \cdot 10^{-3}$ m has to be used. In Fig. 11 (lower panel), the modelled friction velocities at 2.8 m are compared to observed friction velocity and it is clear that even though the larger z_0 reproduce the velocity turning in the upper layer, it overestimates the friction velocity, whereas the modelled friction velocity using $z_0 = 1.3 \cdot 10^{-5}$ m fits the observed friction velocity fairly well. This indicates that the ice at the measurement

site was smoother than the surrounding ice and measurements made at 2.8 m only reflect the local ice topography and are not representative of the entire floe.

Stratification will also affect the velocity profile. A temporal more stable stratification will reduce the eddy viscosity and increase the angular turning with depth, while an unstable stratification will have the opposite effect. Such temporal changes in stratification are likely to occur when drifting over changing water masses as in P2D2 and this is illustrated by comparing two separate periods from this drift. In Fig. 12 average velocity profiles for two 24 hours periods are plotted together with the modelled velocity profile for the same periods using the measured $z_0 = 1.3 \cdot 10^{-5}$ m. The first period (225 – 226, Fig. 12A) is characterized by a stable stratification in the mixed layer and relatively low current speeds ($\overline{N}^2 = -2 \cdot 10^{-5} s^{-1}, \overline{U} = 0.15 ms^{-1}$), whereas the second period (227.5 – 228.5, Fig. 12B) has weaker stratification and higher current speeds ($\overline{N}^2 = -6 \cdot 10^{-6} s^{-1}, \overline{U} = 0.27 ms^{-1}$). Although the angular turning from 3 m to 29 m is comparable fro the two periods, we see from Fig. 12 that for 225 – 226 most of the angular shear is in the upper 15 m, whereas for the second period the angular shear is more or less constant for the depth range examined.

Modelled and observed friction velocity, eddy viscosity and fluxes of heat and salt are plotted in Fig. 13 and mean values are summarized in Table 1. Heat fluxes in the model were calculated according to (4) and they generally show a good agreement with the measured heat fluxes with a mean of 31.5 W m^{-2} versus 28 W m^{-2} for the measured TIC fluxes. As discussed in section 4.2, heat fluxes in the period of 227.5 – 228.5 were higher than expected from the bulk formulation (4) which also indicates that other processes are at play as well. Modelled salt fluxes are calculated from the enthalpy balance at the interface, using excess/deficit heat to melt/freeze ice and calculate a salt/buoyancy flux based on preset ice salinity, which in the model is set to 10 psu. The result of this is that for all heat fluxes larger than the prescribed conductive heat flux in the ice (40 W m^{-2}), ice will melt and result in positive salt fluxes. The overall mean modelled salt flux is roughly comparable to the measured (-1.3·10^{-6} vs. -3.9·10^{-6}), however the modelled salt flux is a result of a pure thermodynamic process at the ice/ocean interface, whereas the measured fluxes are most likely affected by other processes as well, which will be discussed in section 4.5. So even if they compare in magnitude, governing processes are not the same and fluxes can not be compared directly. The modelled eddy viscosity at 2.8 m is plotted in Fig. 13, together with $K_m = u_* \lambda$ calculated from the TIC measurements.

4.5 Effects of horizontal inhomogeniety

Despite the general assumption of horizontal homogeneity when considering turbulence dynamics, it is clear that a strong tidal signal or changes in hydrography over a relatively short horizontal scale affects mixed layer dynamics and introduce extra uncertainty into the calculations of fluxes and turbulent energy. *Crawford et al.* [1999] observed how a lateral salinity gradient was advected by the tide, representing a horizontal buoyancy flux which could both reduce or enhance vertical mixing. Other studies [*Rippeth et al.*, 2001; *Stacey and Ralston*, 2005] showed the importance of the horizontal density gradient on the stratification and turbulence in a bottom boundary layer under a regular semidiurnal tidal flow. In case of *Stacey and Ralston* [2005], the presence of a horizontal density gradient introduced a buoyancy production which, in periods of strong flow, was up to 50% of the shear production, i.e. an important term in the overall TKE budget.

When ice advects through a horizontal salinity gradient, boundary-layer shear will induce a vertical gradient. If, for example, salinity increases in the direction of drift, advection of relatively fresh water near the ice/water interface will induce stable stratification, suppressing turbulence. The opposite situation is illustrated in Fig. 14. With the negative horizontal salinity gradient, in a frame of reference attached to the ice, the mixed layer will appear to freshen faster at depth. If the initial vertical salinity gradient was zero (S_h in Fig. 14), the resulting gradient (S_{adv}) will be statically unstable and provide an additional source of turbulent energy. A horizontal density gradient will also affect the mixed layer dynamics by setting up a vertical gradient in horizontal velocity to balance the horizontal pressure gradient. This baroclinic component will adjust the velocity profile by adding a cross-drift component to the flow in the mixed layer.

Another source of horizontal inhomogeniety is the presence of leads. During winter, leads will be areas of rapid cooling and freezing and hence areas of convection. If the ice is not drifting or only moving slowly, dense plumes will enter the mixed layer as free convection. But more common, when ice is drifting, convecting plumes tend to be dispersed out over a larger area and the effect of convection will be seen as an excess of dissipation rate of TKE.

In order to investigate the effects of horizontal inhomogeniety, we calculate the horizontal density gradient $\frac{\partial \rho}{\partial x} = \frac{1}{U} \frac{\partial \rho}{\partial t}$ from cycling CTD data and depth averaged mixed layer velocity from the ADP profiles (Fig. 15). As expected from the changing hydrography,

$\dfrac{\partial \rho}{\partial x}$ is varying in magnitude and sign with large excursions around 225.5 and 226.7. The period 227.5 – 228.5, which we suspected to be influenced by horizontal inhomogeniety, has the smallest horizontal gradients. However, the gradient remains negative for the entire period, hence this period has the largest average gradient during the drift. This period also has a less stratified mixed layer and a significant vertical velocity (Fig. 15). In addition, there are several other factors that point towards and influence of horizontal inhomogeniety in this period: i) Heat fluxes higher than expected from friction velocities and mixed layer temperatures; ii) Large negative salt fluxes, although heat fluxes indicate melting at the ice/ocean interface, hence positive salt fluxes iii) Increased mixing lengths and weaker stratification iv) A distinct gap between shear production and dissipation indicating an additional source of energy.

We follow the approach of *Simpson et al.* [1990] and calculate the buoyancy production due to a horizontal density gradient as

$$B_h = -\frac{1}{\rho}\left(\frac{\partial \rho}{\partial t}\right)_{adv} = -\frac{1}{\rho}\frac{g}{h}\frac{\partial \rho}{\partial x}\int_{-h_{ml}}^{0}[u(z)-\bar{u}]z\,dz \qquad (11)$$

where $\dfrac{\partial \rho}{\partial x}$ is the horizontal density gradient, $u(z)$ the velocity profile and $\bar{u}$ the depth averaged velocity in the mixed layer. B_h is a depth averaged buoyancy production and not directly comparable to the local TKE terms at 2.8 m. But most of the velocity shear is in the upper meters of the mixed layer and since this will be most of the contribution to B_h, a "local" comparison can be justified.

For the period 227.5 – 228.5, B_h has an average value of $2 \cdot 10{-}8$ m^{2}s^{-3} which is an order of magnitude less than the discrepancy between dissipation rate and shear production and about half of the contribution from the salt flux in the same period. This shows that differential advection of a horizontal density gradient is an order of magnitude too small to be a key driver of turbulence under the encountered conditions or that the applied parameterization, adapted from estuarine conditions, do not sufficiently resolve the important dynamics of the under-ice boundary layer. The largest contribution to the discrepancy in TKE terms observed in 227.5 – 228.5 is believed to come from the increasing amount of leads towards the end of P2D2. However, buoyancy production from horizontal advection can in shorter periods enter the TKE budget as a significant factor.

Usually, an observed effect of convective mixing is deepening of the mixed layer [e.g. *Shay and Gregg*, 1986]. For the period 227.5 – 228.5 this is not observed, h_{ml} is rather constant or even decreasing slightly (Fig. 15). During periods with destabilizing horizontal buoyancy fluxes, *Stacey and Ralston* [2005] observed velocity profiles with maximum within the boundary layer instead of at the top of the boundary layer. For drifting sea ice, a velocity maximum within the mixed layer will modify the effect of horizontal advection of salt. As sketched in Fig. 14, a negative horizontal salinity gradient will lead to a stable stratification below the depth of maximum velocity (h_{Vmax}) in contrast to the unstable stratification above. For the P2D2 drift, mixed layer relative currents from the ADP are decomposed along the direction of the ice drift and h_{Vmax} is found as the depth where this component has its maximum. H_{Vmax} is plotted in Fig. 15 and shows that there were periods where the depth of maximum velocity was within the mixed layer. This was the case for the period 227.5 – 228.5; H_{Vmax} was shallower than h_{ml}, which would prevent deepening of the mixed layer, according to the gradients depicted in Fig. 14. This is also confirmed by the mid-level mast at 30.6 m, which was below h_{Vmax} and had salt fluxes of the opposite sign of the 2.8 m salt fluxes.

The effect of the horizontal density gradient on the velocity profile is investigated by calculating the vertical velocity gradient from the thermal wind equations and the horizontal density gradient:

$$\frac{\partial v}{\partial z} = -\frac{g}{\rho_0 f} \frac{\partial \rho}{\partial x} \tag{12}$$

By integrating (12) over the range of the ADP measurements (3 m to 29 m), the cross-drift velocity component due to the horizontal density gradient is found. This component is then rotated into the East-North reference frame and subtracted from the ADP velocity vectors to find the "true" vectors without influence of horizontal gradients. Angular turning from 3 m to 29 m is then recalculated within every 3 hours intervals and averaged for the entire P2D2 drift and for the two periods 225 – 226 and 227.5 - 228.5. Values are summarized in Table 2. Over the entire drift, the thermal wind contribution reduces the angular turning of velocity by less than 2 degrees and does not seem to be important for the average P2D2 velocity profile. Angular turning is also slightly reduced for the 227.5 – 228.5 period, whereas the largest effect was found for the period 225 – 226. This period also had large horizontal density gradients for shorter periods which certainly affected the velocity profile. Calculations from

the SLTC model are also found in Table 2 and it shows that for the periods 225 - 226 and 227.5 – 228.5, the resulting velocity profiles after correcting for thermal wind seem to be close to the predicted velocity profiles. When plotting the angular turning vs. depth (Fig. 16), this interpretation is repeated for the periods 225 – 229 (entire P2D2 drift) and 227.5 – 228.5. For 225 – 226 it is clear that most of the angular shear is in the upper 15 m, with a revered shear below and even though the model reproduce the "correct" angular shear from 3 m to 29 m, it does not reproduce the angular shear in the upper 15 m. For the 227.5 – 228.5 period the correction for thermal winds seem to adequately account for initial mismatch in angular turning between the measured and modelled velocity profile.

5 Summary

During the two drifts P2D1 and P2D2 on top and on the flank of the Maud Rise, respectively, the following characteristics of the ice and the under ice boundary layer were found:

1. Ice was drifting with an average speed of 3.7 % and 2.6 % of the wind speed, respectively and drift directions were on average 16° and 9° to the left of the wind. In general, the mixed layer oscillated in phase with the ice at the inertial frequency. However, for P2D2, baroclinic flow components were visible in the lower mixed layer due to horizontal gradients in density. From TIC measurements 2.8 m below the ice, LOW calculations indicated roughness lengths of $1.0 \cdot 10^{-6}$ m and $1.3 \cdot 10^{-5}$ m, less than would be expected if the surface was hydraulically smooth. Comparison with SLTC model results indicated that the measurements at 2.8 m were not representative of the surrounding floe.

2. Heat fluxes were 13.8 W m^{-2} and 28.0 W m^{-2} for P2D1 and P2D2, both slightly smaller than estimated conductive heat flux in the ice which indicates that freezing did take place at the interface to balance heat fluxes. No significant changes in ice thickness were observed, however average salt fluxes of $1.0 \cdot 10^{-8}$ psu m s^{-1} and $-1.3 \cdot 10^{-6}$ psu m s^{-1} were measured for P2D1 and P2D2, respectively. Linear regression of kinematic heat flux against the product of friction velocity and mixed layer temperature elevation above freezing, resulted in an average heat transfer coefficient of 0.0059 ± 0.0008 for both drifts, excluding the period susceptible for effects of horizontal inhomogeniety.

3. Mixing length seemed to be limited by the vertical distance from the ice/ocean interface for both drifts. However, for low friction velocities, the planetary length scale seems to be an important scale for turbulence. Towards the end of P2D2, convective events and weak stratification increased the mixing length which in this period is larger than the geometrically limited length scale.

4. In this paper, several factors point towards an influence of a horizontal density gradient, amongst others a discrepancy between shear production and dissipation rate of TKE. The most important potential source of additional TKE are found to be convective leads upstream of the measurement site, however convective mixing caused by differential advection of a negative horizontal density gradient is also believed to be important when ice is drifting through changing water masses.

5. A steady state local turbulence closure model is set up based on temperature and salinity profiles and matched with the measured velocity at 20 m depth. On average, the model reproduces the observed average fluxes, but fails to reproduce some of the variability because i) the model is one dimensional and do not include effects of horizontal inhomogenities and ii) measurements at 2.8 m are to close to the ice/ocean interface to be representative for the floe average and therefore not directly comparable to model results

The results presented here give a picture of the delicate balance of wind, ice, dynamics and thermodynamics in the Antarctic air/sea/ice interaction. The relatively weak pycnocline makes heat transfer from the warm deeper layer to the mixed layer effective and variable; mixing in the surface layer is highly set by the wind forced ice drift, also largely varying in speed and direction. This interplay includes processes that on average can be simulated using relatively simple steady state models and sufficiently long averaging periods. However, on shorter time scales, other processes make the picture more complex.

The effect of differential advection of a horizontal density gradient has been explored in more controlled environments, e.g. in estuaries with a strong tidal currents. This study suggests that these effects can be important also for the boundary layer under drifting sea ice, especially in "inhomogeneous" areas such as the Weddell Sea where both oceanographic and meteorological forcings have high temporal and spatial variability. To further resolve these processes will require continued and more focussed studies in the important areas of air/sea/ice interaction.

Acknowledgments

References

Akitomo, K. (2006), Thermobaric deep convection, baroclinic instability, and their roles in vertical heat transport around Maud Rise in the Weddell Sea, *J Geophys Res-Oceans*, *111*(C9),

Carsey, F. D. (1980), Microwave Observation Of The Weddell Polynya, *Monthly Weather Review*, *108*(12), 2032-2044,

Crawford, G., L. Padman, and M. McPhee (1999), Turbulent mixing in Barrow Strait, *Cont Shelf Res*, *19*(2), 205-245,

de Steur, L., D. M. Holland, R. D. Muench, and M. G. McPhee (2007), The Warm-Water "Halo" around Maud Rise: Properties, Dynamics and Impact, *Deep Sea Research Part I: Oceanographic Research Papers*, *54*(6), 871-896,

Edson, J. B., C. W. Fairall, P. G. Mestayer, and S. E. Larsen (1991), A Study of the Inertial-Dissipation Method for Computing Air-Sea Fluxes, *J Geophys Res-Oceans*, *96*(C6), 10689-10711,

Gordon, A. L. (1978), Deep Antarctic Convection West Of Maud Rise, *J Phys Oceanogr*, *8*(4), 600-612,

Gordon, A. L., and B. A. Huber (1990), Southern-Ocean Winter Mixed Layer, *J Geophys Res-Oceans*, *95*(C7), 11655-11672,

Gordon, A. L. (1991), Two stable modes og Southern Ocean winter stratification, in *Deep Convection and Deep Water Formation in the Oceans*, edited by P. C. Chu and J. C. Gascard, pp. 17-35, Elsevier, Amsterdam.

Hinze, J. O. (1959), *Turbulence*, 586 pp., McGraw-Hill, New York.

Martinson, D. G., and C. Wamser (1990), Ice Drift And Momentum Exchange In Winter Antarctic Pack Ice, *J Geophys Res-Oceans*, *95*(C2), 1741-1755,

McPhee, M. (1990), Small-scale processes, in *Polar Oceanography*, edited by W. Smith, pp. 287-334, Academic Press, San Diego.

McPhee, M., and J. H. Morison (2001), Under-ice boundary layer, in *Encyclopedia of Ocean Sciences*, edited by M. Steele, et al., Academic Press, San Diego.

McPhee, M. G. (1992), Turbulent Heat-Flux in the Upper Ocean under Sea Ice, *J Geophys Res-Oceans*, *97*(C4), 5365-5379,

McPhee, M. G. (1994), On the Turbulent Mixing Length in the Oceanic Boundary-Layer, *J Phys Oceanogr*, *24*(9), 2014-2031,

McPhee, M. G., and D. G. Martinson (1994), Turbulent Mixing under Drifting Pack Ice in the Weddell Sea, *Science*, *263*(5144), 218-221,

McPhee, M. G., S. F. Ackley, P. Guest, B. A. Huber, D. G. Martinson, J. H. Morison, R. D. Muench, L. Padman, and T. P. Stanton (1996), The Antarctic Zone Flux Experiment, *Bull. Amer. Meteorol. Soc.*, *77*(6), 1221-1232,

McPhee, M. G., and T. P. Stanton (1996), Turbulence in the statically unstable oceanic boundary layer under Arctic leads, *J Geophys Res-Oceans*, *101*(C3), 6409-6428,

McPhee, M. G., C. Kottmeier, and J. H. Morison (1999), Ocean heat flux in the central Weddell Sea during winter, *J Phys Oceanogr*, *29*(6), 1166-1179,

McPhee, M. G. (2000), Marginal thermobaric stability in the ice-covered upper ocean over Maud Rise, *J Phys Oceanogr*, *30*(11), 2710-2722,

McPhee, M. G. (2002), Turbulent stress at the ice/ocean interface and bottom surface hydraulic roughness during the SHEBA drift, *J Geophys Res-Oceans*, *107*(C10),

McPhee, M. G. (2008a), Physics of early summer ice/ocean exchanges in the western Weddell Sea during ISPOL, *Deep Sea Research Part II: Topical Studies in Oceanography*, *55*(8-9), 1075 -1097, doi:10.1016/j.dsr2.2007.12.022.

McPhee, M. G. (2008b), *Air-Ice-Ocean interaction: Turbulent Boundary Layer Exchange Processes*, 215 pp., Springer, New York.

McPhee, M. G., J. H. Morison, and F. Nilsen (2008), Revisiting heat and salt exchange at the ice-ocean interface: Ocean flux and modeling considerations, *J Geophys Res*, doi:10.1029/2007JC004383, in press.,

Morison, J., R. Andersen, N. Larson, E. Dasaro, and T. Boyd (1994), The Correction For Thermal-Lag Effects In Sea-Bird Ctd Data, *Journal Of Atmospheric And Oceanic Technology*, *11*(4), 1151-1164,

Muench, R. D., J. H. Morison, L. Padman, D. Martinson, P. Schlosser, B. Huber, and R. Hohmann (2001), Maud Rise revisited, *J Geophys Res-Oceans*, *106*(C2), 2423-2440,

Rippeth, T. P., N. R. Fisher, and J. H. Simpson (2001), The cycle of turbulent dissipation in the presence of tidal straining, *J Phys Oceanogr*, *31*(8), 2458-2471,

Robertson, R., L. Padman, and G. Egbert (1998), Tides in the Weddell Sea, in *Ocean, Ice, and Atmosphere: Interactions at the Antarctic Continental Margin*, edited by S. Jacobs and R. Weiss, pp. 341 - 369, AGU, Washington DC.

Shay, T. J., and M. C. Gregg (1986), Convectively driven turbulent mixing in the oceanic buoyndary layer, *J Phys Oceanogr*, *16*(11), 1777-1798,

Simpson, J. H., J. Brown, J. Matthews, and G. Allen (1990), Tidal Straining, Density Currents, And Stirring In The Control Of Estuarine Stratification, *Estuaries*, *13*(2), 125-132,

Smith, S. D. (1988), Coefficients For Sea-Surface Wind Stress, Heat-Flux, And Wind Profiles As A Function Of Wind-Speed And Temperature, *J Geophys Res-Oceans*, *93*(C12), 15467-15472,

Stacey, M. T., and D. K. Ralston (2005), The scaling and structure of the estuarine bottom boundary layer, *J Phys Oceanogr*, *35*(1), 55-71,

Sturm, M., J. Holmgren, M. Konig, and K. Morris (1997), The thermal conductivity of seasonal snow, *Journal Of Glaciology*, *43*(143), 26-41,

Trodahl, H. J., S. O. F. Wilkinson, M. J. McGuinnes, and T. G. Haskell (2001), Thermal Conductivity of Sea Ice; Dependence on Temperature and Depth, *Geophysical Research Letters*, *28*(7), 1279-1282,

Widell, K., I. Fer, and P. M. Haugan (2006), Salt release from warming sea ice, *Geophysical Research Letters*, *33*(12),

Zwally, H. J., and P. Gloersen (1977), Passive microwave images of the polar regions and research applications, *Polar Rec.*, *18*, 431-450,

Tables

Table 1 Mean values of friction velocity, heat flux, salt flux and eddy viscosity for both drifts. TIC values are measured at 2.8 m below the ice, model values are from the SLTC model. For P2D2 the model and the TIC measurements cover the same period, for P2D1 TIC measurements were from day 221.9 – 222.8 and model values from day 222.6 – 223.3. TIC salt fluxes (F_s) are from μC (upper) and stdC (lower) sensors.

	u_* [cms^{-1}]		F_H [Wm^{-2}]		F_S [psu ms^{-1}]		K_m [m^{2}s^{-1}]	
	TIC	Model	TIC	Model	TIC	Model	TIC	Model
P2D1	1.00	-	13.8	-	$2.1 \cdot 10^{-8}$	-	0.0081	-
P2D2	0.56	0.57	28.0	31.5	$-3.8 \cdot 10^{-6}$	$-1.3 \cdot 10^{-6}$	0.0044	0.0063
					$-3.9 \cdot 10^{-6}$			

Table 2 Angular turning of the mean velocity vector from 3m to 29m calculated from 3 hours averages for the entire P2D2 period, 225 – 226 and 227.5 – 228.5. In the second and third column, horizontal density gradients and vertical gradients of the cross-drift velocity component are given. The fourth column shows turning of velocity after subtracting the thermal wind component within every averaging interval. In the last column velocity turning from the idealized SLTC model is given.

Period	Angle, $V_{29m} - V_{3m}$	$\partial \rho / \partial x$ kg m^{-4}	$\partial v / \partial z$ s^{-1}	Angle, $V_{29m} - V_{3m}$ corrected for thermal wind	Angle, $V_{29m} - V_{3m}$ from SLTC model
All	12.3°	$-2.61 \cdot 10^{-6}$	$1.9 \cdot 10^{-4}$	10.6°	5.6°
225 – 226	12.0°	$-1.24 \cdot 10^{-5}$	$9.1 \cdot 10^{-4}$	4.7°	5.8°
227.5 – 228.5	9.7°	$-3.96 \cdot 10^{-6}$	$2.9 \cdot 10^{-4}$	6.7°	7.1°

Figures
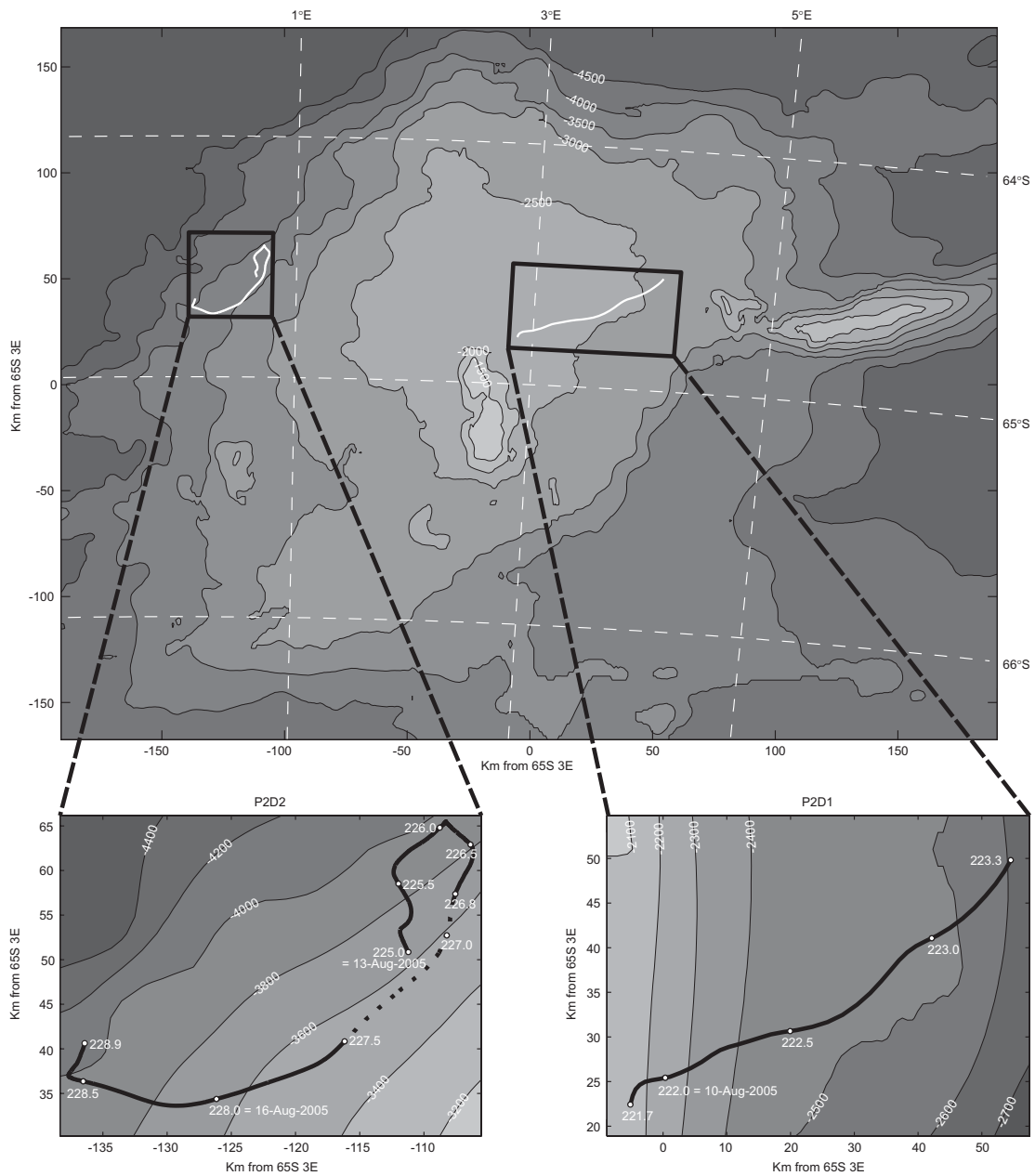
Fig. 1 Upper panel shows the bathymetry of the Maud Rise from the GEBCO bathymetry (Reproduced from the GEBCO Digital Atlas published by the British Oceanographic Data Centre on behalf of IOC and IHO, 2003) in a polar stereographic grid centred at 65S 3E. Drift trajectories are plotted on top and magnified in the lower panels together with time stamps. The dashed line in the P2D2 trajectory indicates when the instruments were relocated.
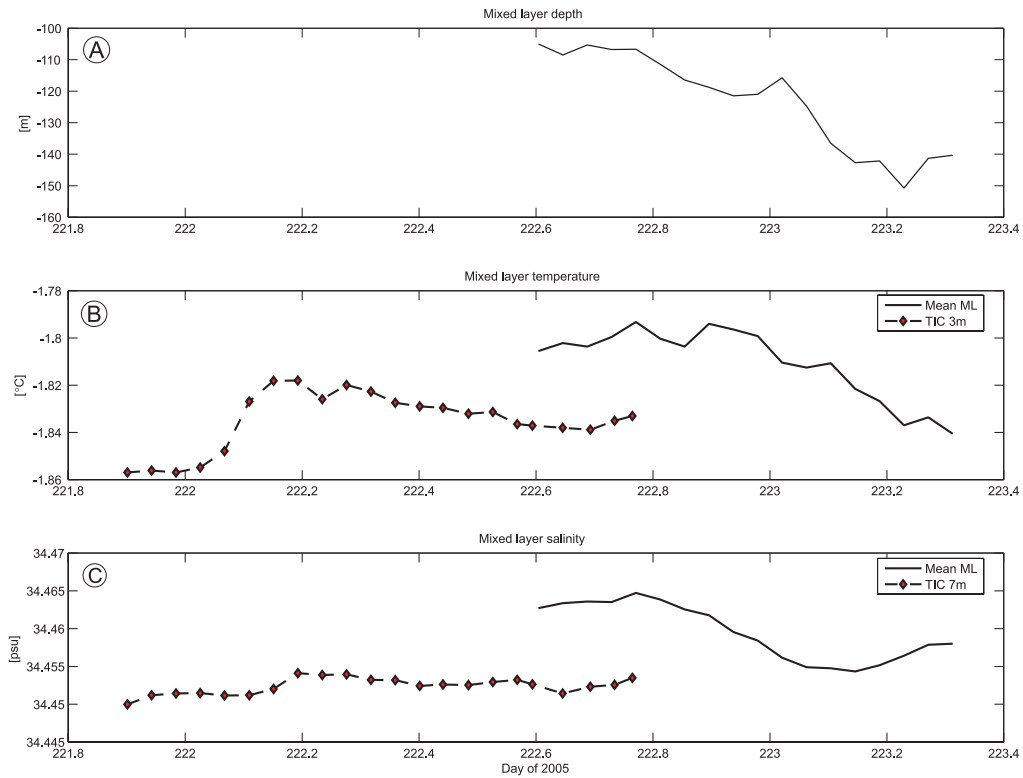
Fig. 2 Mixed layer depth (A), mixed layer temperature (B) and mixed layer salinity (C) for the P2D1 drift. TIC values (diamonds) are hourly average values from 3m below the ice for temperature and 7m below the ice for salinity. The "mean ML" values are hourly values from the yoyo CTD and are the average of all measurements within the mixed layer.
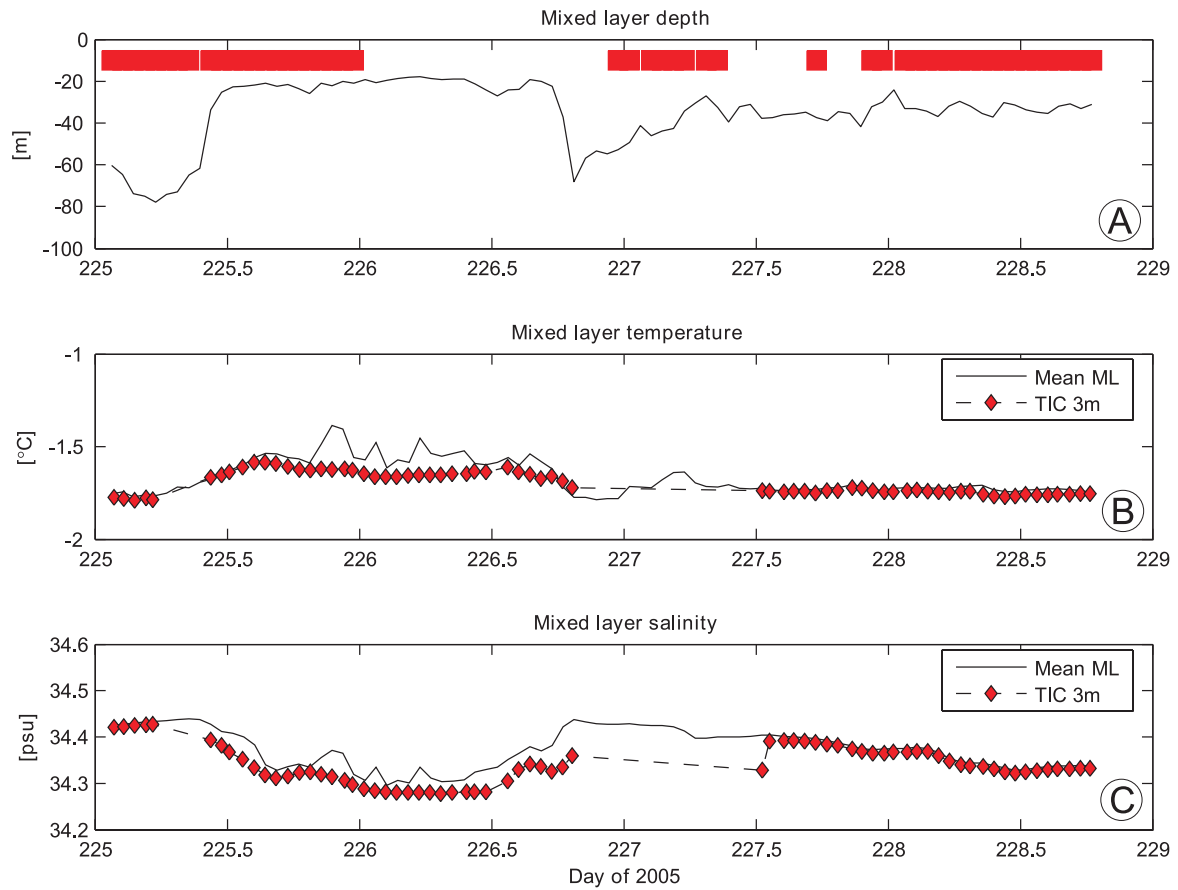
Fig. 3 Mixed layer depth (A), mixed layer temperature (B) and mixed layer salinity (C) for the P2D2 drift. TIC values (diamonds) are hourly average values from 3m below the ice for temperature and salinity. Red markers in upper panel indicate when the water column has Halo Water properties ($T_{max}>1°C$, $S_{max}>34.7$). The "mean ML" values are hourly values from the yoyo CTD and are the average of all measurements within the mixed layer.
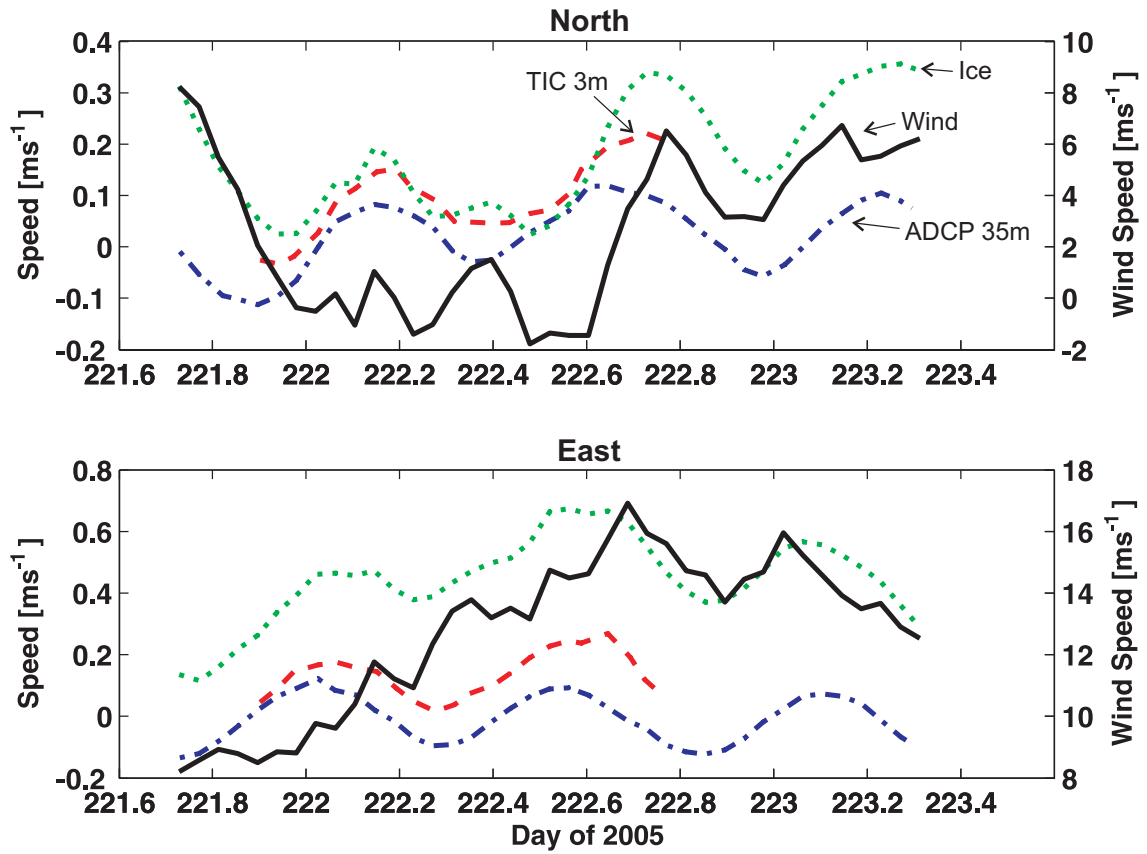
Fig. 4 North and east components of absolute velocities including the wind speed at 10 m height (solid line), ice drift velocity (dashed line), current velocity from the TIC at 3m depth (dashed-dotted line) and the velocity at 35m depth as measured by the nb150 ADCP (dotted line). Wind speed scale on right.
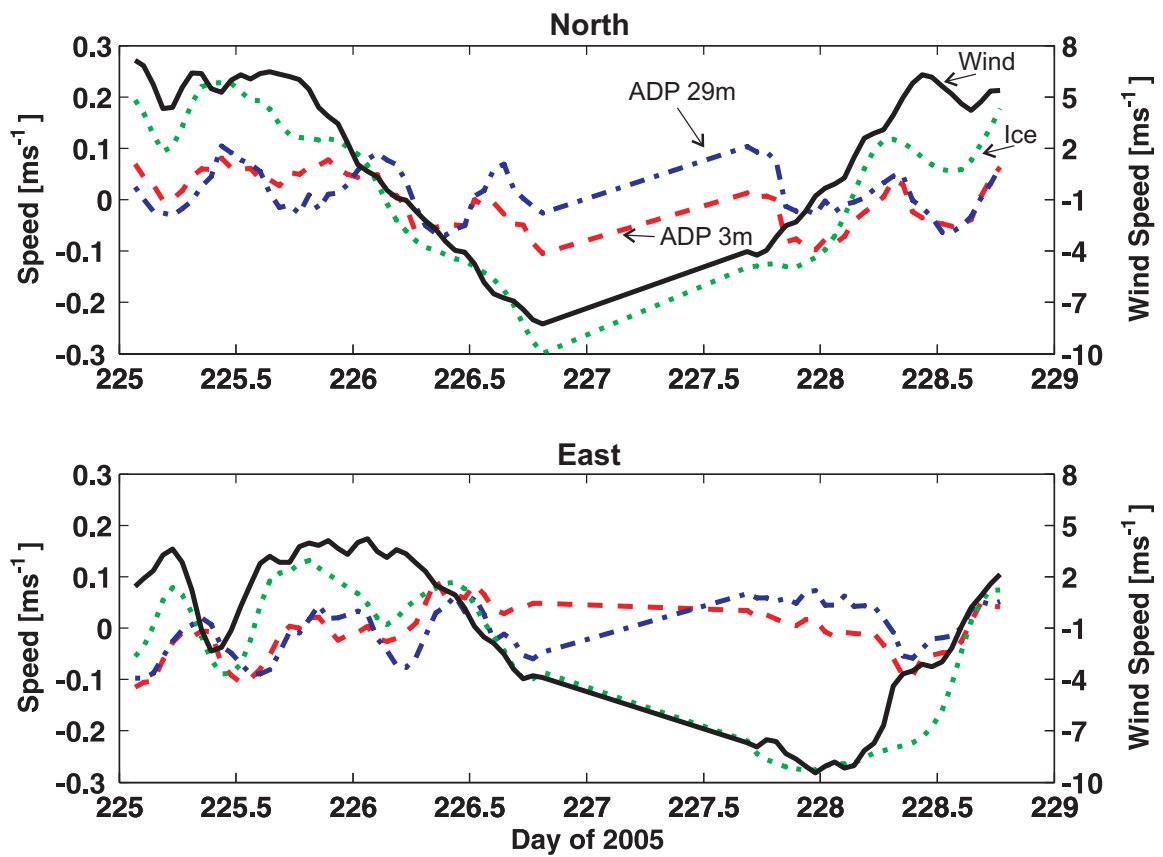
Fig. 5 North and east components of absolute velocities including the wind speed at 10 m height (solid line), ice drift velocity (dashed line), current velocity from the ADP at 3m depth (dashed-dotted line) and the velocity at 29 m depth as measured by the ADP (dotted line). Wind speed scale on right.
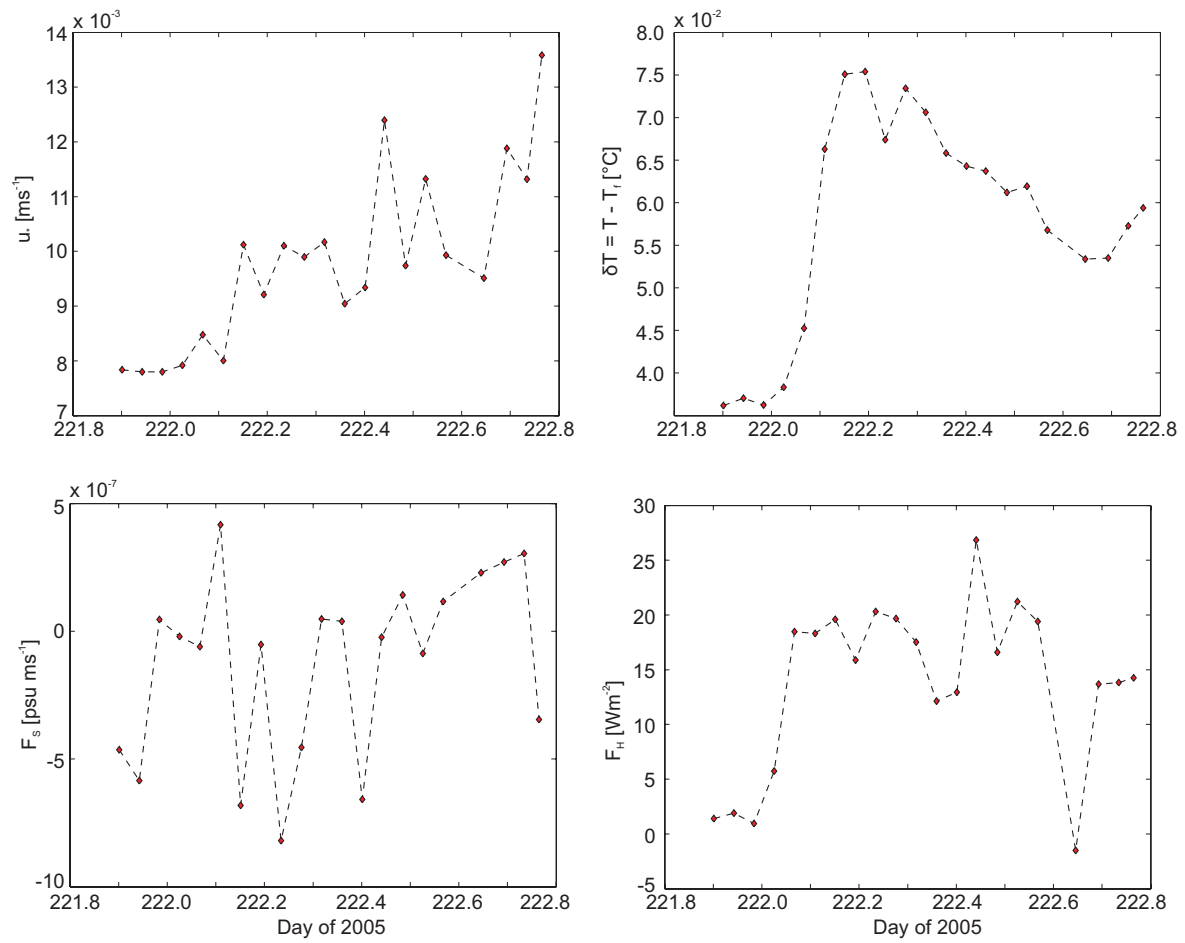
Fig. 6 Friction velocity (upper left), temperature elevation above freezing (upper right), salt flux (lower left) and heat flux (lower right) for the P2D1 drift. All values are hourly means measured by the TIC at 3 m depth, except the salt flux which is measured at 7 m depth.
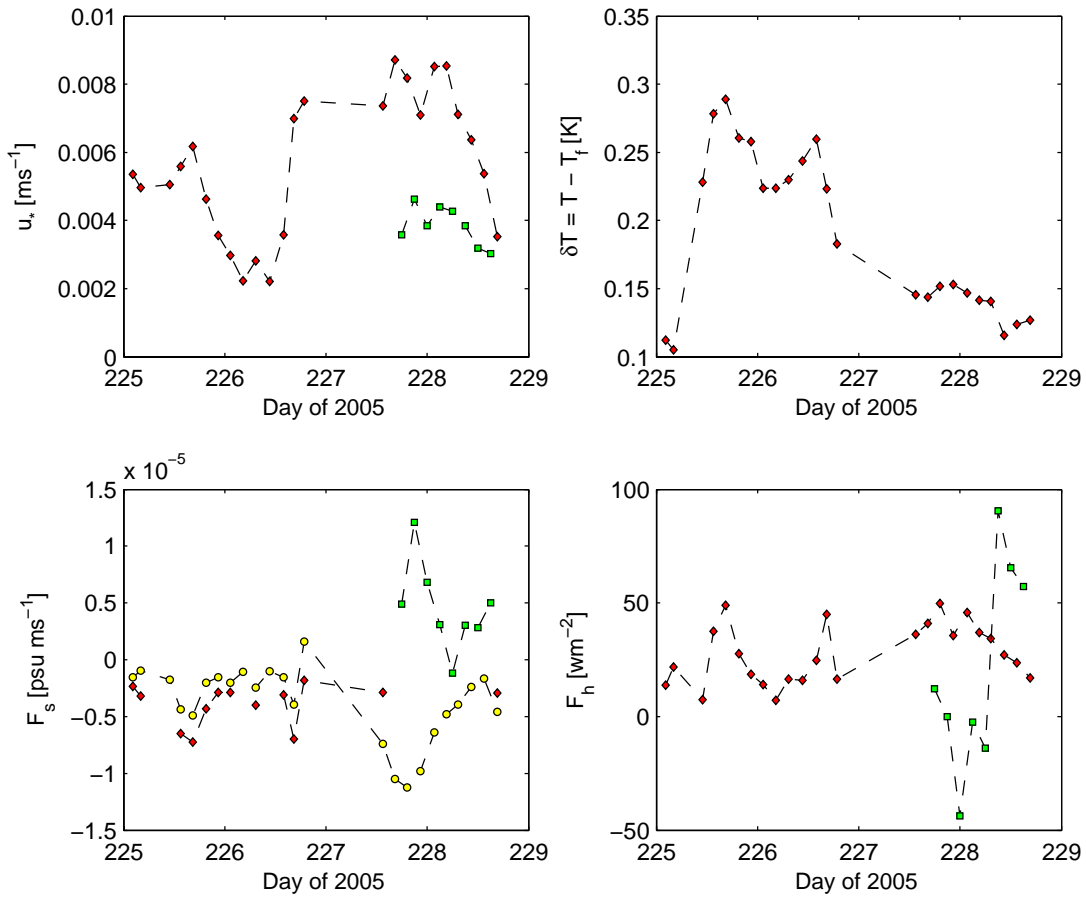
Fig. 7 Friction velocity (upper left), temperature elevation above freezing (upper right), salt flux (lower left) and heat flux (lower right) measured at 3 m depth for the P2D2 drift. Squares are values from the mid-depth mast at 30.6 m and for the salt flux (lower left), circles indicate flux from μC sensor, diamonds are values from stdC sensor and squares are fluxes from the mid-level mast at 30 m depth.
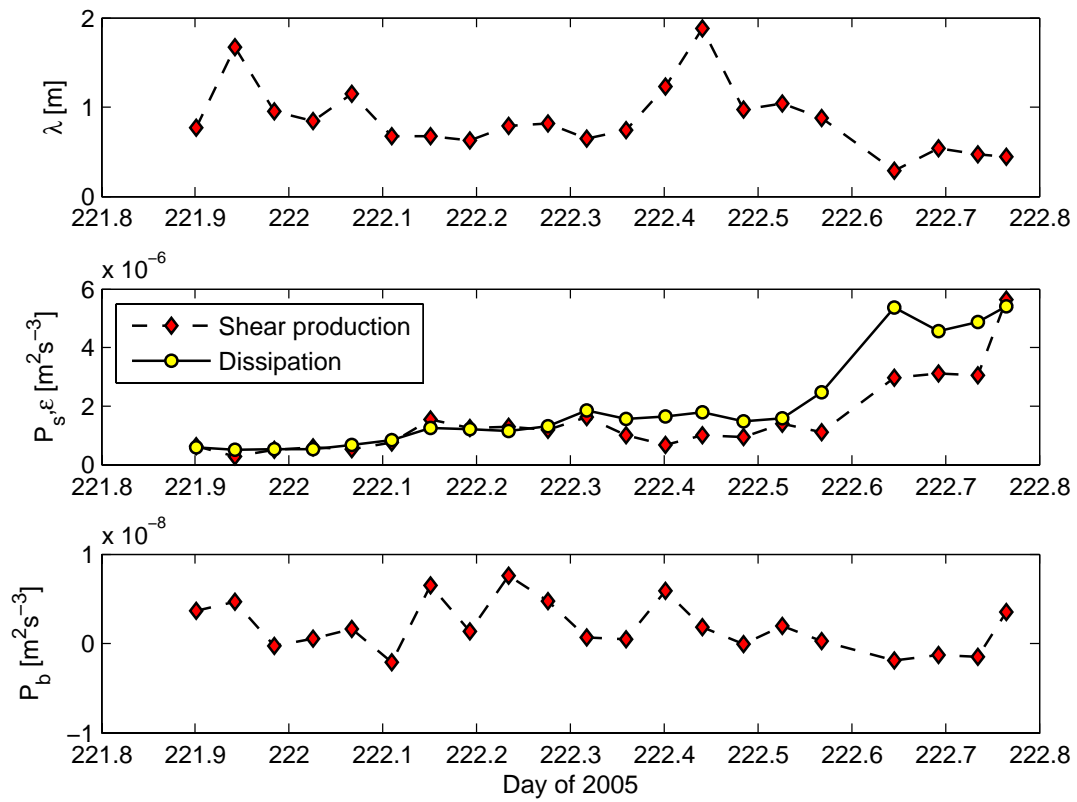
Fig. 8 TKE terms for the P2D1 drift. Mixing length as calculated from the w' spectra (upper panel), shear production (middle panel, dashed line + diamonds) and dissipation (middle panel, solid line + circles) and buoyancy production (lower panel) inferred from the turbulent salt flux measured at 6.8 m depth. All values are hourly averages.
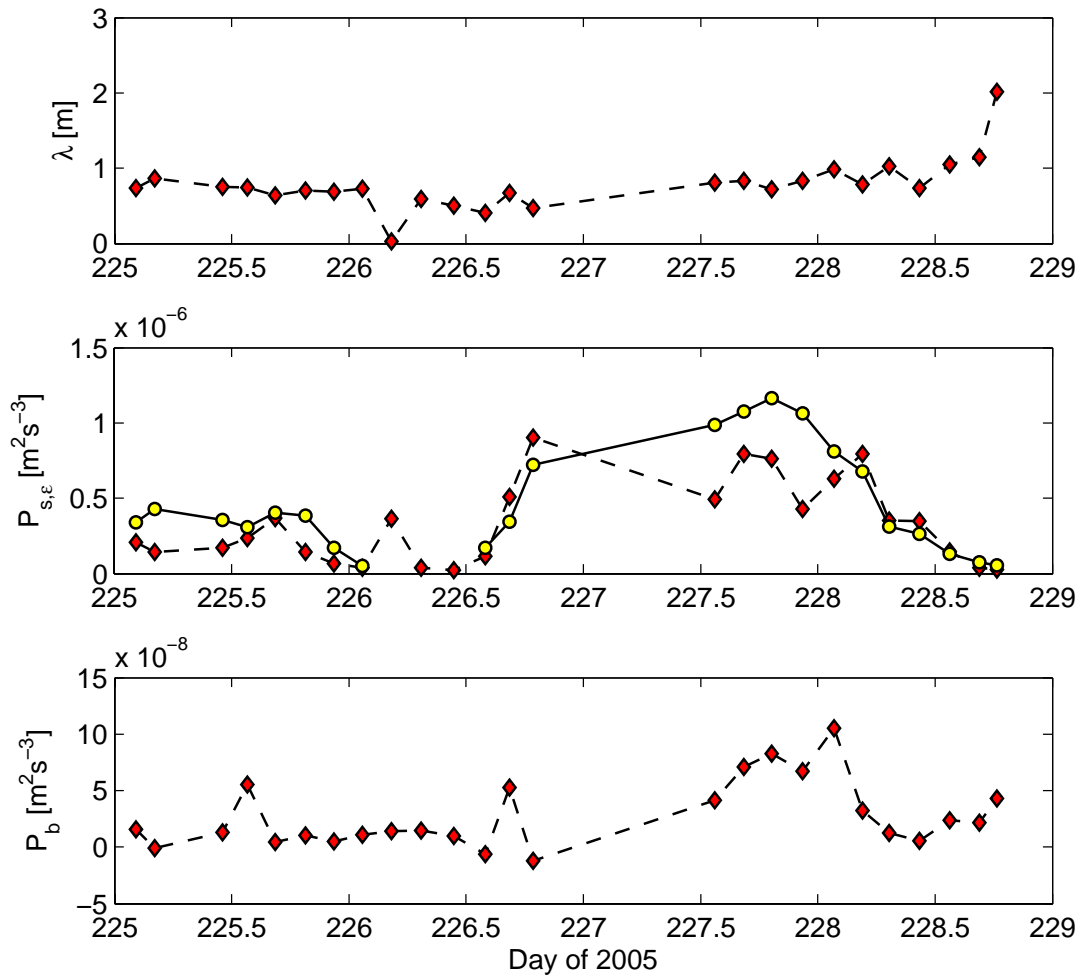
Fig. 9 TKE terms for the P2D2 drift. Mixing length as calculated from the w' spectra (upper panel), shear production (middle panel, dashed line + diamonds) and dissipation (middle panel, solid line + circles) and buoyancy production (lower panel) inferred from the turbulent salt flux. All values are three hours averages.
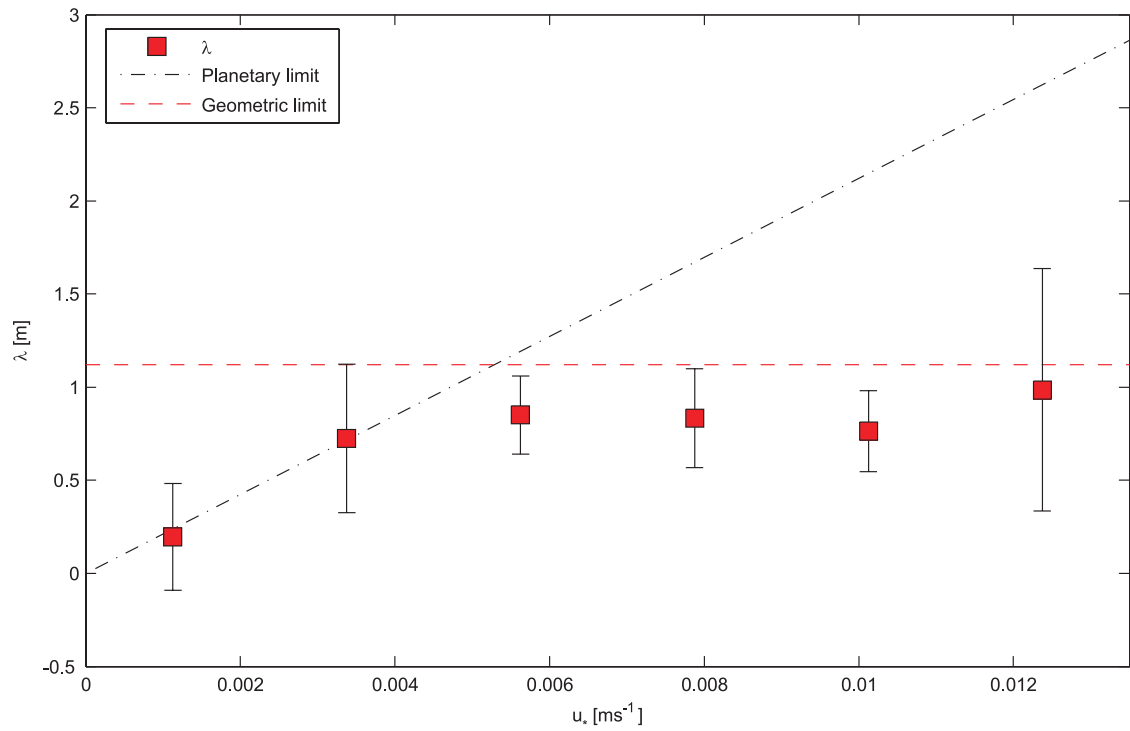
Fig. 10 Hourly values of mixing length plotted against friction velocity for both drifts. Values are averaged in bins of friction velocity of $1.5 \cdot 10^{-3}$ ms^{-1}. The dashed horizontal line is the geometric limit for mixing length in the surface layer and dashed-dotted line is the planetary limit.
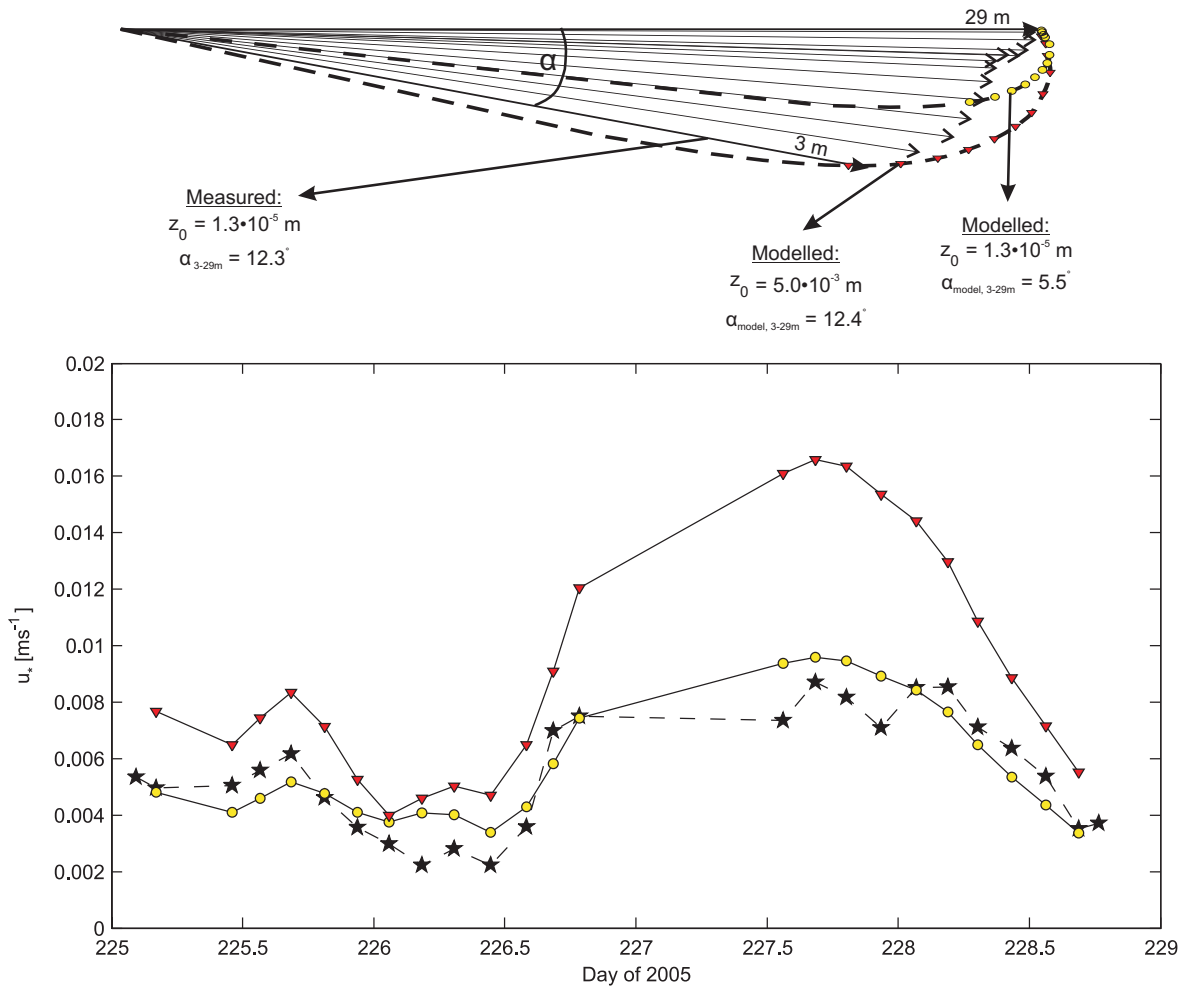
Fig. 11 Arrows in the upper panel shows the relative velocity in the depth interval 3 m to 29 m non dimensionalized by the velocity at 29 m as mean over the whole drift. Plotted circles on top are the corresponding velocities from the same depths as calculated using the SLTC model with specified roughness lengths of $1.3 \cdot 10^{-5}$ m (circles) and $5 \cdot 10^{-3}$ m (triangles), respectively. Angles of turning from 3 m to 29 m are given. Lower panel shows the modelled friction velocities at cluster depth (2.8 m) for the two different roughness lengths compared with the measured friction velocity (stars).
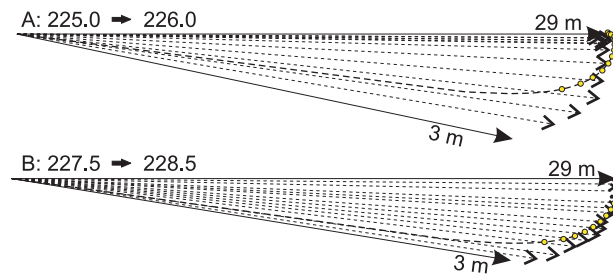
Fig. 12 Upper panel: Relative velocities non dimensionalized by the velocity at 29m (arrows) for the period 225 – 226. Lower panel is the same; however velocities are averaged over period 227.5 to 228.5. In both panels the average velocity profile from the model for each period calculated using the average surface roughness $z_0=1.3·10^{-5}$m is overlaid.
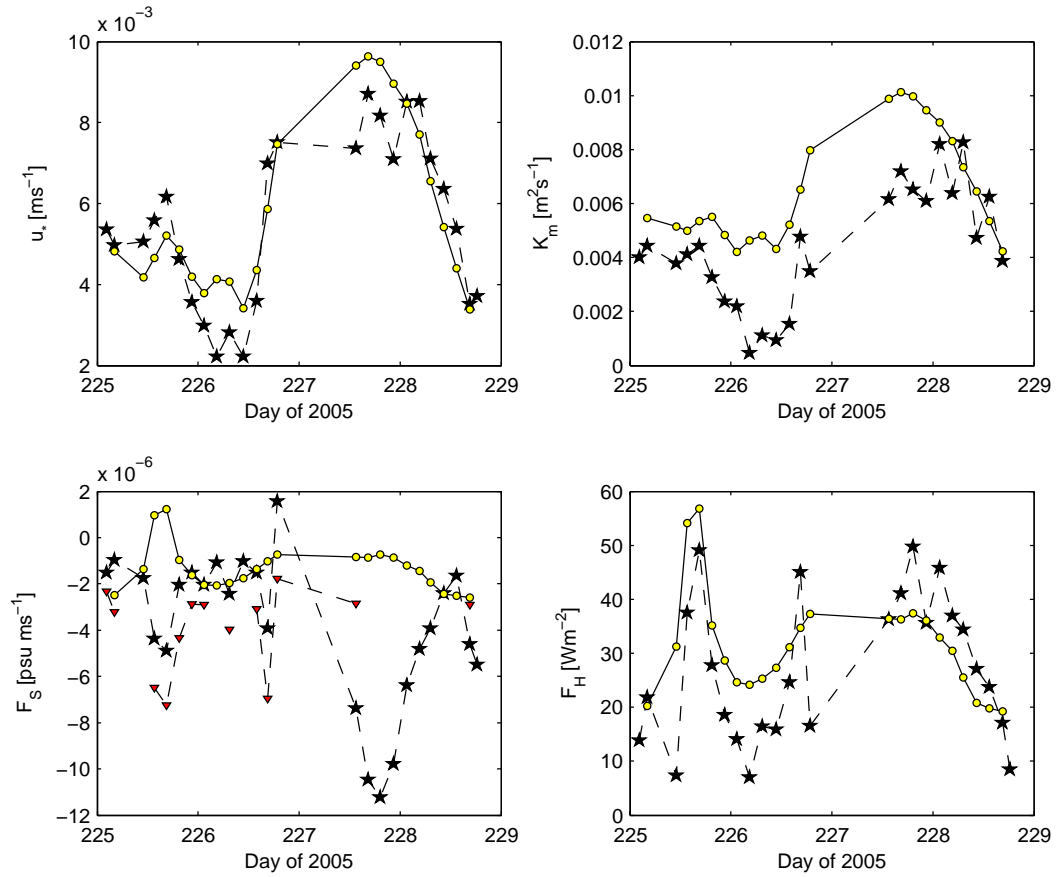
Fig. 13 Comparison of modelled (circles) and measured (stars) friction velocity, heat flux , salt flux and eddy viscosity for the P2D2 drift at depth 2.8 m. Modelled fluxes are found using roughness length 1.3·10⁻⁵ m. In lower left panel, stars indicate the μC saltflux and triangles indicate stdC salt fluxes. All values are three hours averages.
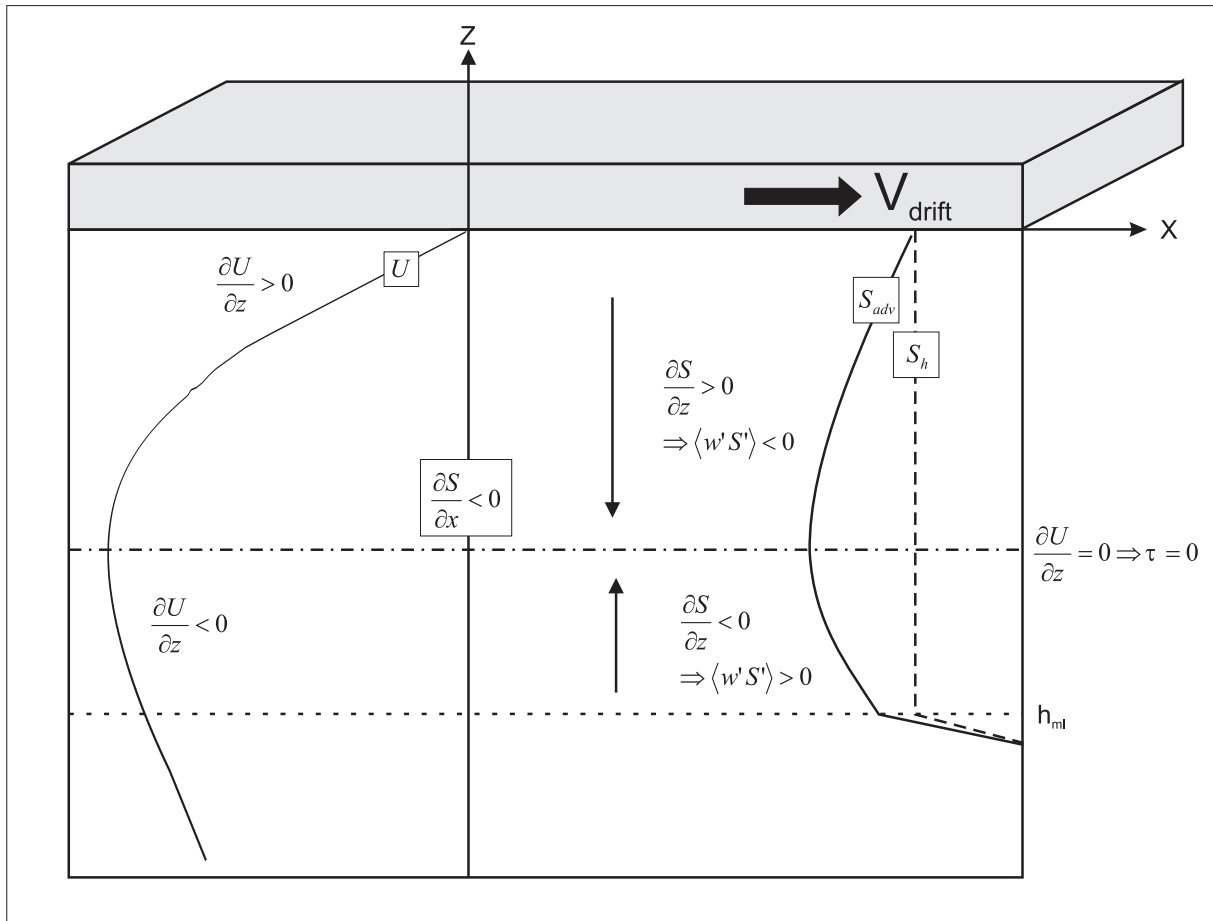
Fig. 14 Schematic sketch of process of horizontal advection. U is the along drift velocity, S_h is the salinity in case of horizontally homogeneous conditions and S_{adv} is the salinity in case of horizontal advection with S_h as initial condition.
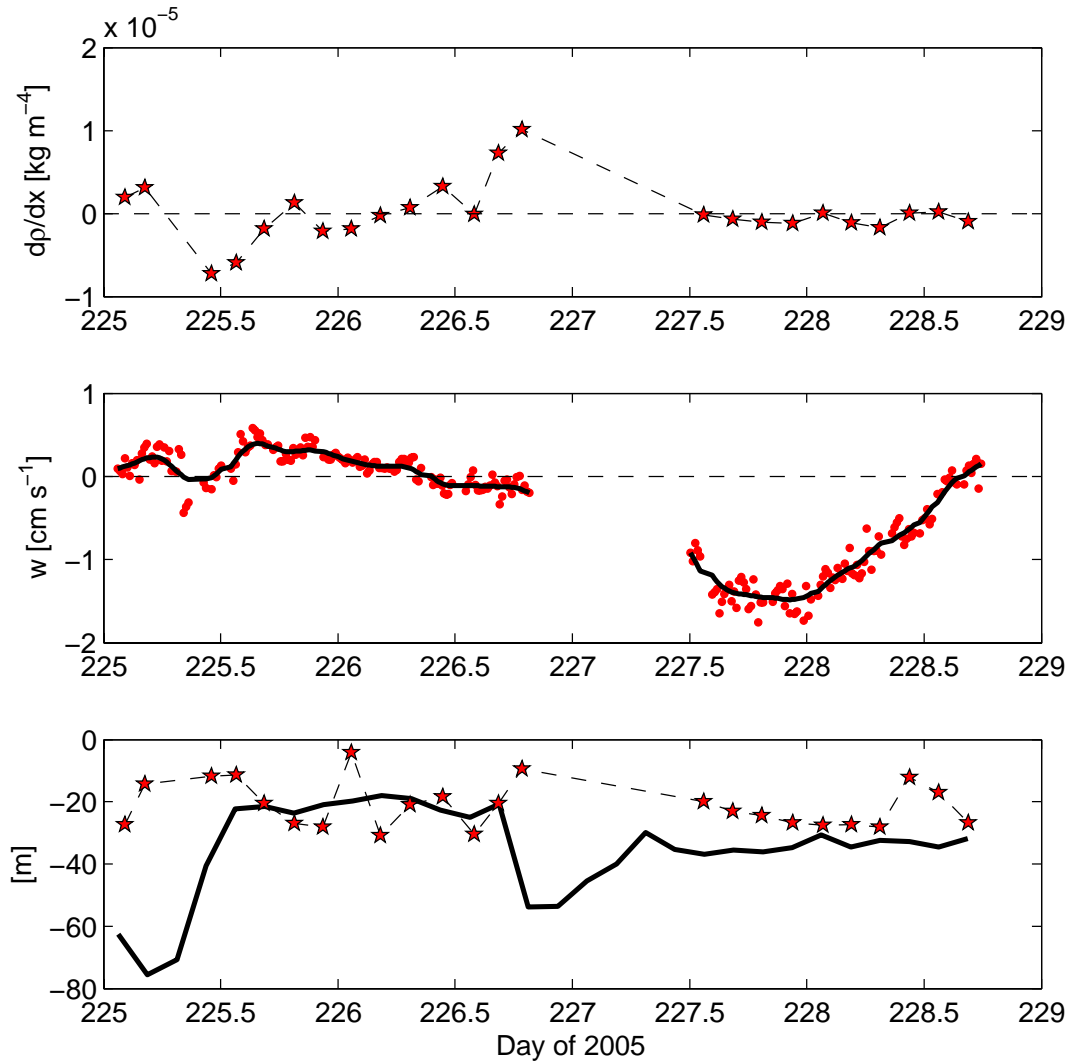
Fig. 15 Upper panel shows three hours averages of horizontal density gradient. Middle panel shows the vertical velocity at 2.8 m depth, dots are 15 min values and thick line is a three hours running mean and lower panel shows three hours averages of mixed layer depth calculated from the yoyo data (solid line) and the depth of maximum velocity from the ADP data (pentagrams).
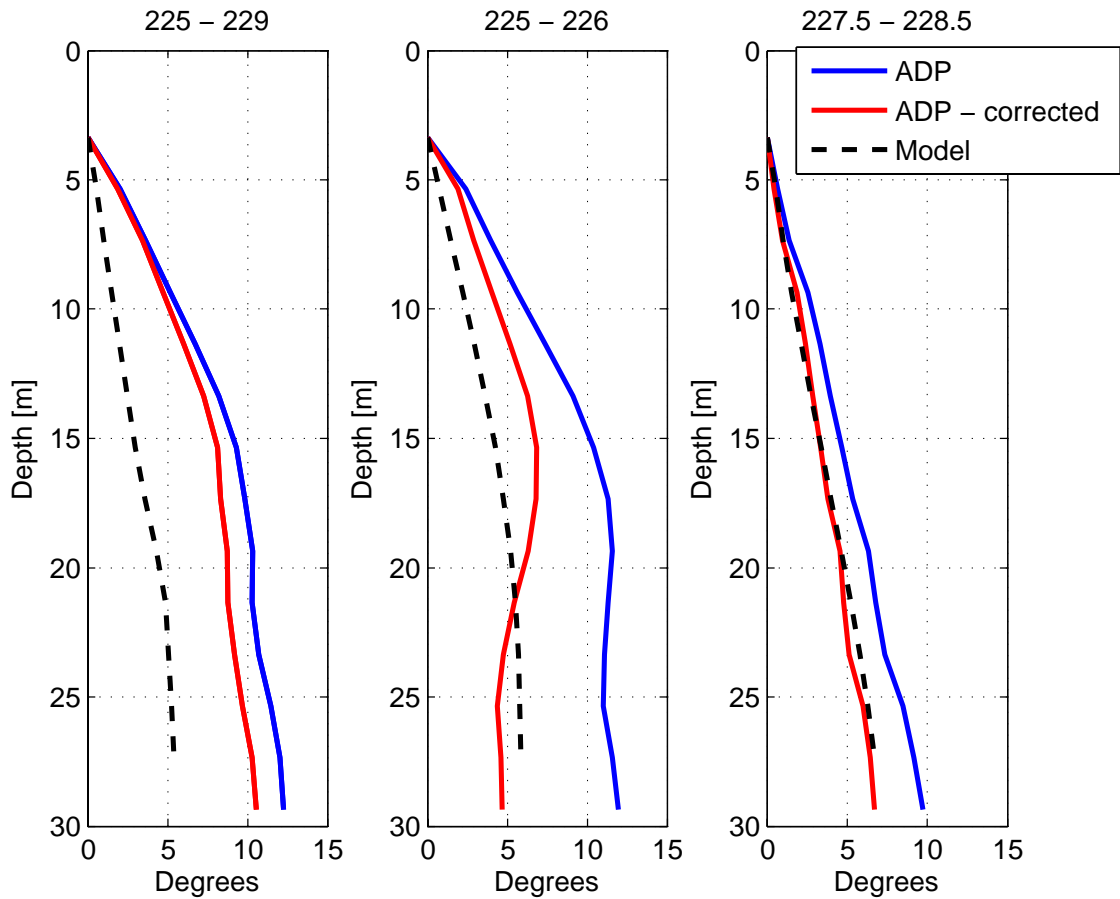
Fig. 16 Figure shows the average angular turning of the velocity vector from 3 m to 29 m for the entire P2D2 drift (left), 225 – 226 (middle) and 227.5 – 228.5 (right). Blue lines are angular turning as measured with the ADP, red lines are also ADP measurements but corrected for the thermal wind effect and dashed lines are the estimated angular turning from the SLTC model.